

# Using Spin Correlations to Distinguish $Zh$ from $ZA$ at the International Linear Collider

Gregory Mahlon\*

*Penn State Mont Alto*

*1 Campus Drive, Mont Alto, PA 17237*

*USA*

Stephen Parke†

*Department of Theoretical Physics*

*Fermi National Accelerator Laboratory*

*P.O. Box 500, Batavia, IL 60510*

*USA*

(Dated: June 5, 2006)

## Abstract

We investigate how to exploit the spin information imparted to the  $Z$  boson in associated Higgs production at a future linear collider as an aid in distinguishing between  $CP$ -even and  $CP$ -odd Higgs bosons. We apply a generalized spin-basis analysis which allows us to study the possibilities offered by non-traditional choices of spin projection axis. In particular, we find that the  $Z$  bosons produced in association with a  $CP$ -even Higgs via polarized collisions are in a single transverse spin-state ( $> 90\%$  purity) when we use the  $Zh$ -transverse basis, provided that the  $Z$  bosons are not ultra-relativistic (speed  $< 0.9c$ ). This same basis applied to the associated production of a  $CP$ -odd Higgs yields  $Z$ 's that are an approximately equal mixture of longitudinal and transverse polarizations. We present a decay angular distribution which could be used to distinguish between the  $CP$ -even and  $CP$ -odd cases. Finally, we make a few brief remarks about how this distribution would be affected if the Higgs boson turns out to not be a  $CP$ -eigenstate.

---

\*Electronic address: gdm10@psu.edu

†Electronic address: parke@fnal.gov

## I. INTRODUCTION

One of the goals of high energy physics during the next decade is to elucidate the mechanism for the spontaneous symmetry breaking in the electroweak sector. In the Standard Model, this symmetry breaking leaves behind a single Higgs boson with spin-parity-charge-conjugation quantum numbers  $\mathcal{J}^{PC} = 0^{++}$ . As soon as a Higgs candidate is discovered, we will want to examine it closely to see if its properties match those of the Standard Model, or, if not, which extension to or replacement of the Standard Model is implied. For example, supersymmetric theories contain a  $0^{+-}$  state alongside of a SM-like  $0^{++}$  boson; certain other models add a  $Z'$  boson (spin-1) to the mix. Thus, the direct determination of the  $\mathcal{J}^{PC}$  assignment for a newly-discovered boson will be a priority. There are at least different three ways of constraining the quantum numbers of such a boson. First, we can examine the energy-dependence of the associated production cross section just above threshold [1]. Second, we can look at the dependence of the cross section on the production angle [2]. Thirdly, and this is the point of this paper, we can study a suitably-chosen decay-angle distribution. Even though this last method is potentially the most difficult, it will be useful to supplement the other two methods with additional information from angular correlations to resolve possible ambiguities or to provide a cross-check [3].

At first glance, it might seem that since the Higgs ( $\phi$ ) is a spin-0 object, all angular correlations should be trivial. However, this is not the case. For example, the decay products of the tau leptons coming from  $\phi \rightarrow \tau^+\tau^-$  decays exhibit non-trivial correlations that can be used to probe the nature of the Higgs [4]. Similarly, if the decay to a pair of vector bosons exists, then by looking at the angular distributions of the vector boson decay products it is possible to distinguish a  $CP$ -even Higgs boson ( $h$ ) from a  $CP$ -odd Higgs boson ( $A$ ) [2, 5]. These angular distributions are sensitive to the type of Higgs boson involved because of the presence of a  $\phi VV$  vertex in the process. However, this method suffers from the drawback that there is no guarantee that the  $\phi \rightarrow VV$  branching ratio will be large enough to be useful. Fortunately, it is not necessary that  $\phi \rightarrow VV$  exist to probe the properties of the Higgs boson: the so-called associated production mechanism also contains a  $\phi VV$  vertex (see Fig. 1).

Thus, the  $Z$  boson produced in association with the Higgs at a linear collider carries information about the type of Higgs it was produced with. Consequently, by examining the

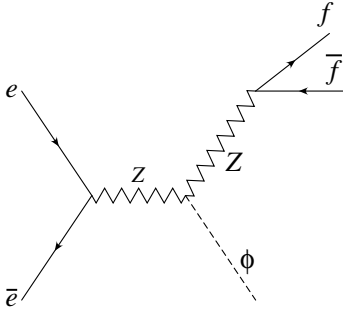


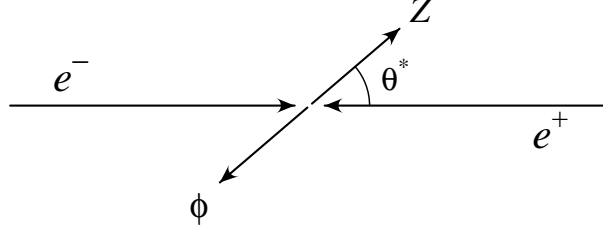
FIG. 1: The Feynman diagram for the production and decay of a Higgs boson ( $\phi$ ) in association with a  $Z$  boson.

spin state of the  $Z$ , we can learn about the Higgs in a model-independent fashion. Since we understand  $Z$  decays very well (see, for example, the review of  $Z$  physics contained in Ref. [6]), any deviations from Standard Model predictions will point to new physics in the Higgs sector.

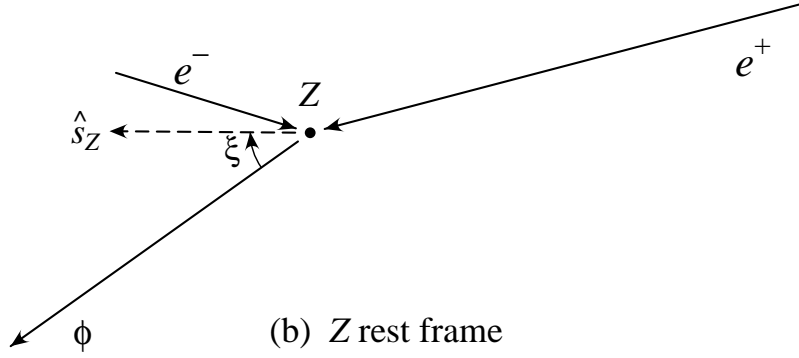
Traditionally, angular correlations have been studied within the context provided by the helicity basis. For a light Higgs and a linear collider running at a full TeV or so, this is appropriate. However, in situations where the  $Z$  boson and Higgs are not ultra-relativistic, the helicity basis may not give the most useful description of the physics involved. Instead, it is fruitful to explore other choices of spin axis [7, 8, 9, 10, 11]. One framework which facilitates this exploration in a fairly straightforward manner is the generic spin basis ( $\xi$ -basis) introduced by Parke and Shadmi in Ref. [8]. One possibility that this framework allows for is the analysis of the data (or independent subsets thereof) in two (or more) different ways, to see if the spin content of the  $Z$  bosons varies with  $\xi$  in the predicted manner.

Spin correlations in associated Higgs production at a hadron collider ( $q\bar{q}' \rightarrow W\phi$ ) have already been studied in Ref. [11]. Angular correlations are most easily observed and understood in the zero momentum frame of the event. At a hadron collider, however, the  $z$  component of the total momentum in the event is ambiguous, making the zero momentum frame difficult to find. We have written this paper from the point-of-view of a future  $e^+e^-$  linear collider to utilize the advantages offered by such a machine. Not only is the zero momentum frame relatively well-known in this case, but the ability to polarize the beams enhances the angular correlations.

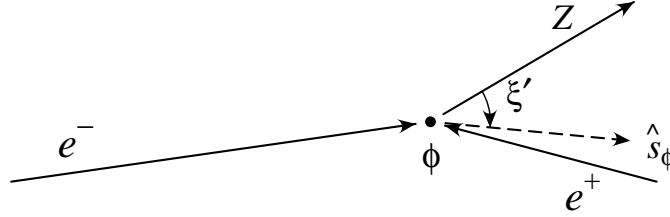
The outline of this paper is as follows. After a brief discussion of our notation and conventions in Sec. II, we present the polarized  $Zh$  and  $ZA$  production cross sections at a linear collider in Sec. III. Next, we turn to a review of the decay distributions ( $Z \rightarrow f\bar{f}$ ) in the case of polarized  $Z$  bosons in Sec. IV. In Sec. V we combine the production and decay amplitudes to derive expressions for the triply-differential cross sections for  $e^+e^- \rightarrow Zh \rightarrow f\bar{f}h$  and  $e^+e^- \rightarrow ZA \rightarrow f\bar{f}A$ , with an emphasis on the forms of these distributions in the helicity and  $Zh$ -transverse bases. Integrating the triply-differential cross section over the production and decay azimuthal angles leads to the principle results of this paper in Sec. VI: the angular distribution  $d\sigma/d(\cos\chi)$  of the  $Z$  boson decay products as seen in the  $Z$  rest frame. We compare this distribution in the  $Zh$  and  $ZA$  cases in Sec. VIE and in Fig. 13. We make a few brief remarks about how this distribution would be different in the case where the Higgs boson is not in a  $CP$ -eigenstate in Sec. VIF. Finally, we end with a summary of our conclusions in Sec. VII.



(a) zero momentum frame



(b) Z rest frame



(c) Higgs rest frame

FIG. 2: The scattering process in (a) the zero momentum frame, (b) the rest-frame of the  $Z$  boson and (c) the rest-frame of the Higgs. The spin axis for the  $Z$  ( $\phi$ ) is  $\hat{s}_Z$  ( $\hat{s}_\phi$ ).

## II. NOTATION AND CONVENTIONS

Throughout this paper, we use the symbol  $\phi$  to refer to a generic Higgs boson which could either be  $CP$  even or  $CP$  odd or have no unique  $CP$  eigenvalue. The symbol  $h$  will be reserved for use when we are talking specifically about a  $CP$ -even Higgs boson. Finally, a  $CP$ -odd Higgs boson will be represented by the symbol  $A$ .

To describe the polarized production cross sections for  $e^+e^- \rightarrow Z\phi$  followed by the subsequent decay of the  $Z$  we adopt the  $\xi$ -basis, introduced by Parke and Shadmi in Ref. [8].

As illustrated in Fig. 2, the zero momentum frame (ZMF) production angle  $\theta^*$  is defined as the angle between the electron and  $Z$  momentum directions. The spin states for the  $Z$  boson are defined in its rest frame, where we decompose its spin along the direction  $\hat{s}_Z$ , which makes an angle  $\xi$  in the clockwise direction from the Higgs momentum. Although our method does not require detailed observation of the Higgs boson decay products, for completeness, we will go ahead and define a Higgs “spin” axis,  $\hat{s}_\phi$ . This unit vector is located at the angle  $\xi'$  in the clockwise direction from the  $Z$  boson momentum. The spin-zero character of the Higgs will be reflected in a lack of any dependence of the amplitudes on the choice of this axis ( $\xi'$ ).

We denote the two transverse polarization states of the  $Z$  boson by  $(\uparrow)$  and  $(\downarrow)$  (or, equivalently,  $(+)$  and  $(-)$  respectively) and the longitudinal state by  $(0)$ . Throughout this paper we use the terms “transverse” and “longitudinal” to refer to directions relative to the spin axis rather than to the direction of motion of the particle. A generic vector boson spin will be designated by  $\lambda$ . If we sum over all of the polarizations of the  $Z$  boson, then the dependence on  $\xi$  drops out of the result.

Within this generic framework, specific spin bases are defined by stating the relationship between  $\xi$ ,  $\theta^*$ , and any other relevant event parameters. For example, the familiar helicity basis is defined by fixing

$$\xi \equiv \pi. \tag{1}$$

In this case, the spin axes are defined along the directions of motion of the particles as seen in the ZMF. Later in this paper, we will encounter additional bases, whose definitions are inspired by the form of the matrix elements for the processes under consideration.

Except for the fermion masses, which we set equal to zero, all input masses and coupling constants used in the computations presented in this paper are the central values as reported in the 2004 Review of Particle Properties [6]. Consistent with the zero fermion mass approximation, we set the coupling between the electron and the Higgs to zero.

### III. ASSOCIATED HIGGS PRODUCTION AT A LINEAR COLLIDER

#### A. Polarized $Zh$ Production

The two particles produced in the process  $e^+e^- \rightarrow Zh$ , being of different masses, will have different speeds in the ZMF. Thus, we may choose to write the amplitudes in terms of the ZMF speed of the  $Z$  boson  $\beta_z$ , or the ZMF speed of the Higgs  $\beta_h$ ; we have chosen to use  $\beta_z$ . In addition to the masses of the Higgs and  $Z$  bosons, the value of  $\beta_z$  also depends on  $\sqrt{s}$ , the center-of-mass energy of the collider:

$$\beta_z = \frac{\sqrt{[s - (M_z + M_h)^2][s - (M_z - M_h)^2]}}{s - M_h^2 + M_z^2}. \quad (2)$$

A plot of  $\beta_z$  as a function of the (still-unknown) value of  $M_h$  for various center-of-mass energies appears in Fig. 3. For reasons of simplicity, we retain both  $s$  and  $\beta_z$  in our expressions rather than using Eq. (2) to eliminate one of them.

If we neglect the electron mass, there is but a single diagram for  $e^+e^- \rightarrow Zh$ , as displayed in Fig. 1 [12]. With the aid of the formalism described in Ref. [7], it is straightforward to calculate the differential cross section for  $Zh$  production using polarized beams where the  $Z$  is in the spin state  $\lambda$ :

$$\frac{d\sigma_L^\lambda(e_L^- e_R^+ \rightarrow Zh)}{d(\cos \theta^*)} = G_F^2 \frac{M_W^2 M_Z^2}{8\pi s} \Theta(s, M_h, M_Z) q_{eL}^2 [\mathcal{S}_L^\lambda(\beta_z, \theta^*, \xi)]^2, \quad (3)$$

$$\frac{d\sigma_R^\lambda(e_R^- e_L^+ \rightarrow Zh)}{d(\cos \theta^*)} = G_F^2 \frac{M_W^2 M_Z^2}{8\pi s} \Theta(s, M_h, M_Z) q_{eR}^2 [\mathcal{S}_R^\lambda(\beta_z, \theta^*, \xi)]^2. \quad (4)$$

In these expressions,  $G_F$  is the Fermi coupling constant,  $M_W$  is the mass of the  $W$  boson, and  $\theta_W$  is the Weinberg angle. The kinematics associated with the threshold behavior of the cross section have been collected into the function  $\Theta(s, M_h, M_Z)$ , which is defined to be

$$\Theta(s, M_h, M_Z) \equiv 2\beta_z \gamma_z \frac{M_Z}{\sqrt{s}} \left( \frac{s + M_Z^2 - M_h^2}{s - M_Z^2} \right)^2. \quad (5)$$

Here  $\sqrt{s}$  is the collider center-of-mass energy,  $\beta_z$  the speed of the  $Z$  boson in the zero momentum frame (ZMF) of the event, and  $\gamma_z$  the usual relativistic boost factor,

$$\gamma_z \equiv (1 - \beta_z^2)^{-1/2}. \quad (6)$$

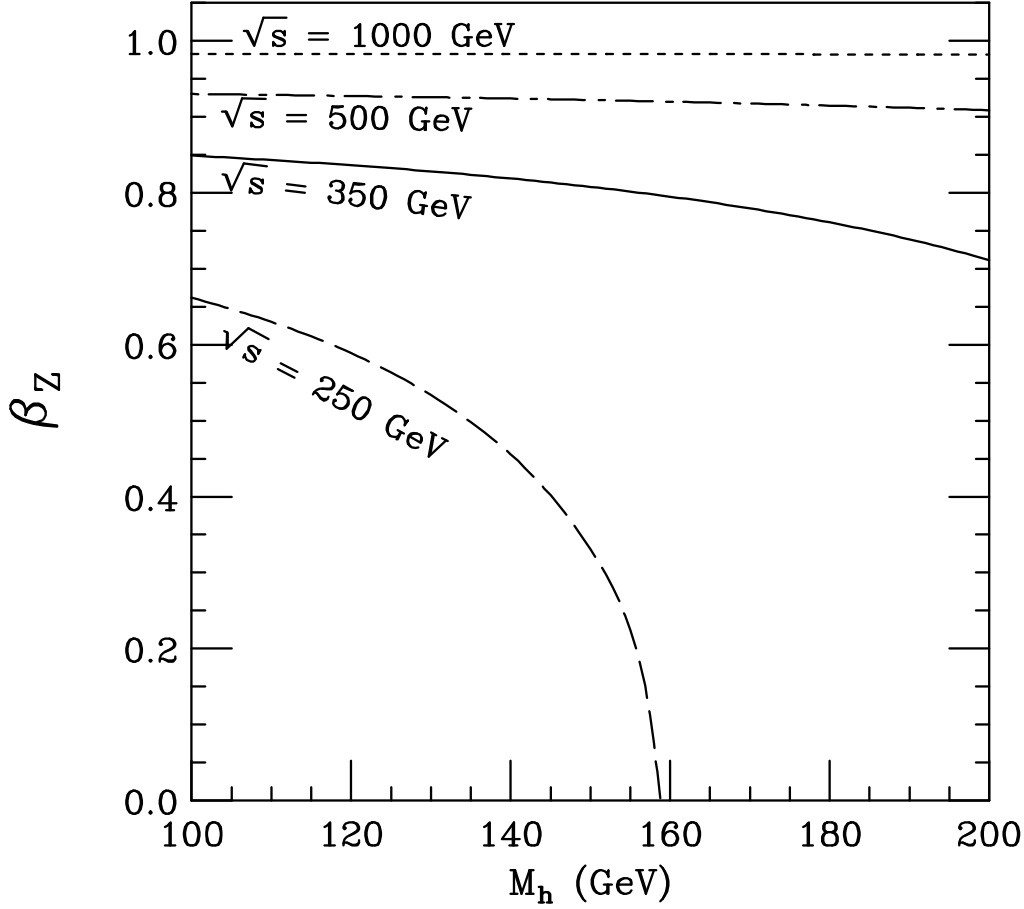


FIG. 3: Zero momentum frame speed of the  $Z$  boson,  $\beta_Z$ , as a function of the Higgs mass in  $e^+e^- \rightarrow Zh$  for collider energies  $\sqrt{s} = 250$  GeV, 350 GeV, 500 GeV, and 1000 GeV.

We have chosen the factors that comprise  $\Theta(s, M_h, M_Z)$  so that for  $\beta_Z \rightarrow 1$  (equivalently,  $s \rightarrow \infty$ ) we have  $\Theta \rightarrow 1$ . Naturally,  $\Theta = 0$  at threshold. We parameterize the  $Zf\bar{f}$  vertex as

$$i\Gamma^\mu \equiv ig \left[ q_{fL} \gamma^\mu \frac{1}{2} (1 - \gamma_5) + q_{fR} \gamma^\mu \frac{1}{2} (1 + \gamma_5) \right]. \quad (7)$$

Here  $g$  is the weak coupling constant; it is connected to the Fermi coupling constant in the usual manner:

$$\frac{G_F}{\sqrt{2}} = \frac{g^2}{8M_w^2}. \quad (8)$$

The quantity  $q_{fL}$  describes the coupling of a left-handed fermion line of flavor  $f$  to the  $Z$  boson while  $q_{fR}$  represents the coupling of the  $Z$  boson to a right-handed fermion line. These couplings are collected in Table I for easy reference. All of the remaining spin information is contained in the spin functions,  $\mathcal{S}_{L,R}^\lambda$ , which, for  $e_L^- e_R^+$ , are given by ( $s_\theta \equiv \sin \theta^*$ ,  $c_\theta \equiv \cos \theta^*$ ,



TABLE I: Standard Model couplings of fermions to the  $Z$  boson. The numerical values correspond to  $\sin^2 \theta_W = 0.2312$ .

fermion	$q_{fL}$	$q_{fR}$
$u, c$	$\frac{(1 - \frac{4}{3} \sin^2 \theta_W)}{2 \cos \theta_W} = .3945$	$\frac{(-\frac{4}{3} \sin^2 \theta_W)}{2 \cos \theta_W} = -.1758$
$d, s, b$	$\frac{(-1 + \frac{2}{3} \sin^2 \theta_W)}{2 \cos \theta_W} = -.4824$	$\frac{(\frac{2}{3} \sin^2 \theta_W)}{2 \cos \theta_W} = .0879$
$e, \mu, \tau$	$\frac{(2 \sin^2 \theta_W - 1)}{2 \cos \theta_W} = -.3066$	$\frac{(2 \sin^2 \theta_W)}{2 \cos \theta_W} = .2637$
$\nu$	$\frac{1}{2 \cos \theta_W} = 0.5702$	0

etc.):

$$\begin{aligned}\mathcal{S}_L^\pm(\beta_z, \theta^*, \xi) &= \frac{1}{\sqrt{2}} \left[ s_\theta s_\xi + \gamma_z^{-1} (c_\theta c_\xi \pm 1) \right]; \\ \mathcal{S}_L^0(\beta_z, \theta^*, \xi) &= \gamma_z^{-1} c_\theta s_\xi - s_\theta c_\xi.\end{aligned}\tag{9}$$

The spin functions for a right-handed electron line are related to the left-handed functions via

$$\begin{aligned}\mathcal{S}_R^\pm(\beta_z, \theta^*, \xi) &= \mathcal{S}_L^\mp(\beta_z, \theta^*, \xi) \\ \mathcal{S}_R^0(\beta_z, \theta^*, \xi) &= \mathcal{S}_L^0(\beta_z, \theta^*, \xi).\end{aligned}\tag{10}$$

To provide some sense of how the polarized production amplitudes depend on our choice of spin basis we now examine the explicit form of these amplitudes in a couple of cases of interest. First, in the helicity basis ( $\xi = \pi$ ) we have

$$\begin{aligned}\mathcal{S}_L^\pm(\beta_z, \theta^*, \pi) &= -\frac{\gamma_z^{-1}}{\sqrt{2}} (c_\theta \mp 1) \\ \mathcal{S}_L^0(\beta_z, \theta^*, \pi) &= s_\theta.\end{aligned}\tag{11}$$

Unless  $\beta_z$  is rather close to 1, one consequence of these expressions is that a non-negligible fraction of the total integrated cross section will be supplied by each of the three spins (see Fig. 5 below). A second consequence of the form of these amplitudes is the equality of the contributions to the total integrated cross section from the (+) and (−) spin components at all values  $\beta_z$ , even for polarized beams (odd functions of  $c_\theta$  drop out when we integrate over  $\cos \theta^*$ ; the only difference between  $|\mathcal{S}_L^+|^2$  and  $|\mathcal{S}_L^-|^2$  is in the sign of the  $\cos \theta^*$  cross term).

We contrast these results with the  $Zh$ -transverse basis, which was introduced in Ref. [7]. This basis was motivated by a desire to eliminate one of the three spin components. Now, according to Eqs. (9) and (10), it is not possible to make both of the spin functions  $\mathcal{S}_L^\lambda$  and  $\mathcal{S}_R^\lambda$  vanish simultaneously when  $\lambda$  is  $(+)$  or  $(-)$ . Consequently, for unpolarized beams, it is impossible to choose a spin basis for which either variety of transversely-polarized  $Z$  boson is absent. On the other hand, it is possible to eliminate the contribution from the longitudinal  $Z$  bosons by choosing

$$s_\xi = \frac{s_\theta}{\sqrt{1 - \beta_z^2 c_\theta^2}}; \quad c_\xi = \frac{\gamma_z^{-1} c_\theta}{\sqrt{1 - \beta_z^2 c_\theta^2}}, \quad (12)$$

which may be abbreviated as

$$\tan \xi = \gamma_z \tan \theta^*. \quad (13)$$

Eq. (12) defines the  $Zh$ -transverse basis, so-called because in this basis only  $Z$ 's with transverse polarizations are produced. Although the choice of  $\xi$  implied by Eq. (12) looks like a radical departure from the simplicity ( $s_\xi = 0$ ;  $c_\xi = -1$ ) of the ZMF helicity basis in that it selects a different spin axis for each event, in reality, the same is true for the choice  $\xi = \pi$ . Recall that  $\xi$  is defined relative to the direction of motion of the  $Z$  boson in the ZMF: this direction is different for each event. What we have done in defining the  $Zh$ -transverse basis is to include some cleverly-selected  $\beta_z$ -dependence in addition to the (now explicit)  $\theta^*$ -dependence. Note that the existence of this basis depends on neither the machine energy nor the Higgs mass: Eqs. (2) and (12) remain well-defined so long as  $\sqrt{s} \geq M_z + M_h$  (*i.e.* a  $Zh$  final state must be kinematically allowed). In particular, for  $\beta_z \rightarrow 1$ , we have

$$s_\xi \rightarrow 1; \quad c_\xi \rightarrow 0, \quad (14)$$

that is,  $\xi \rightarrow \pi/2$ . This is clearly *not* the helicity basis, suggesting that even far above threshold the  $Zh$ -transverse basis represents a different and potentially interesting way of viewing the data. At the other energy extreme,  $\beta_z \rightarrow 0$ , we have

$$s_\xi \rightarrow s_\theta; \quad c_\xi \rightarrow c_\theta. \quad (15)$$

A moment's consideration of Fig. 2 along with Eq. (15) will lead to the recognition that the directions of the incoming beams are being used to decompose the spins in this limit. That is, at threshold, the  $Zh$ -transverse basis is coincident with the so-called beamline basis[9] (see Appendix C).

In addition to eliminating the contribution from the longitudinal spin component, the  $Zh$ -transverse basis is also the basis in which the  $+$  and  $-$  components are each maximized.

In the  $Zh$ -transverse basis, the explicit forms of the spin functions are

$$\begin{aligned}\mathcal{S}_L^\pm(\beta_z, \theta^*, \tan^{-1}(\gamma_z \tan \theta^*)) &= \frac{1}{\sqrt{2}} \left( \sqrt{1 - \beta_z^2 \cos^2 \theta^*} \pm \sqrt{1 - \beta_z^2} \right) \\ \mathcal{S}_L^0(\beta_z, \theta^*, \tan^{-1}(\gamma_z \tan \theta^*)) &= 0.\end{aligned}\tag{16}$$

It is clear from these expressions that the  $(+)$  and  $(-)$  states are equally-populated for polarized beams only in the ultra-relativistic limit ( $\beta_z \rightarrow 1$ ); for small  $\beta_z$ , one of these two states is approximately empty.

In Fig. 4 we display plots of the contributions from the three spin states as a function of the  $Z$  production angle  $\cos \theta^*$  at  $\beta_z = 0.59$ , corresponding to the not-implausible combination  $m_h = 120$  GeV,  $\sqrt{s} = 250$  GeV. These plots clearly exhibit the features noted above: in the helicity basis, all three spin components make significant contributions to the total cross section whereas in the  $Zh$ -transverse basis a single component dominates depending on the polarization of the incoming beams.

Given a choice of basis (i.e.  $\xi$ ) and machine energy (i.e.  $\beta_z$ , once  $M_h$  is known) we may integrate Eqs. (3) and (4) over  $\cos \theta^*$  to determine the fraction of  $Z$  bosons produced in each of the three possible spin states. In Fig. 5 we present the results as a function of  $\beta_z$ ; Table II lists the numerical values corresponding to  $\beta_z = 0.59$ , that is, at the same Higgs mass and machine energy considered in Fig. 4. The fractions in the helicity basis are essentially as anticipated above, starting at an equal mixture of  $(+)$ ,  $(-)$  and  $(0)$  at threshold and becoming 100% longitudinal as  $\beta_z \rightarrow 1$ . At all energies the fractions of  $(+)$  and  $(-)$  spins are equal, even for polarized beams. In contrast, the  $Zh$ -transverse basis fractions are relatively insensitive to  $\beta_z$  (unless  $\beta_z$  gets fairly large).

Summing over the three possible spins of the  $Z$  we obtain the total differential cross section

$$\sum_\lambda \frac{d\sigma_L^\lambda}{d(\cos \theta^*)} = q_{eL}^2 G_F^2 \frac{M_W^2 M_Z^2}{8\pi s} \Theta(s, M_h, M_Z) \left[ 2 - \beta_z^2 (1 + \cos^2 \theta^*) \right].\tag{17}$$

If we replace  $q_{eL}$  by  $q_{eR}$  in Eq. (17) we obtain the result for  $e_R^- e_L^+$  scattering. Eq. (17) is independent of the spin axis angle  $\xi$ , as it must be. This expression corresponds to the curves labeled “TOTAL” in Fig. 4.

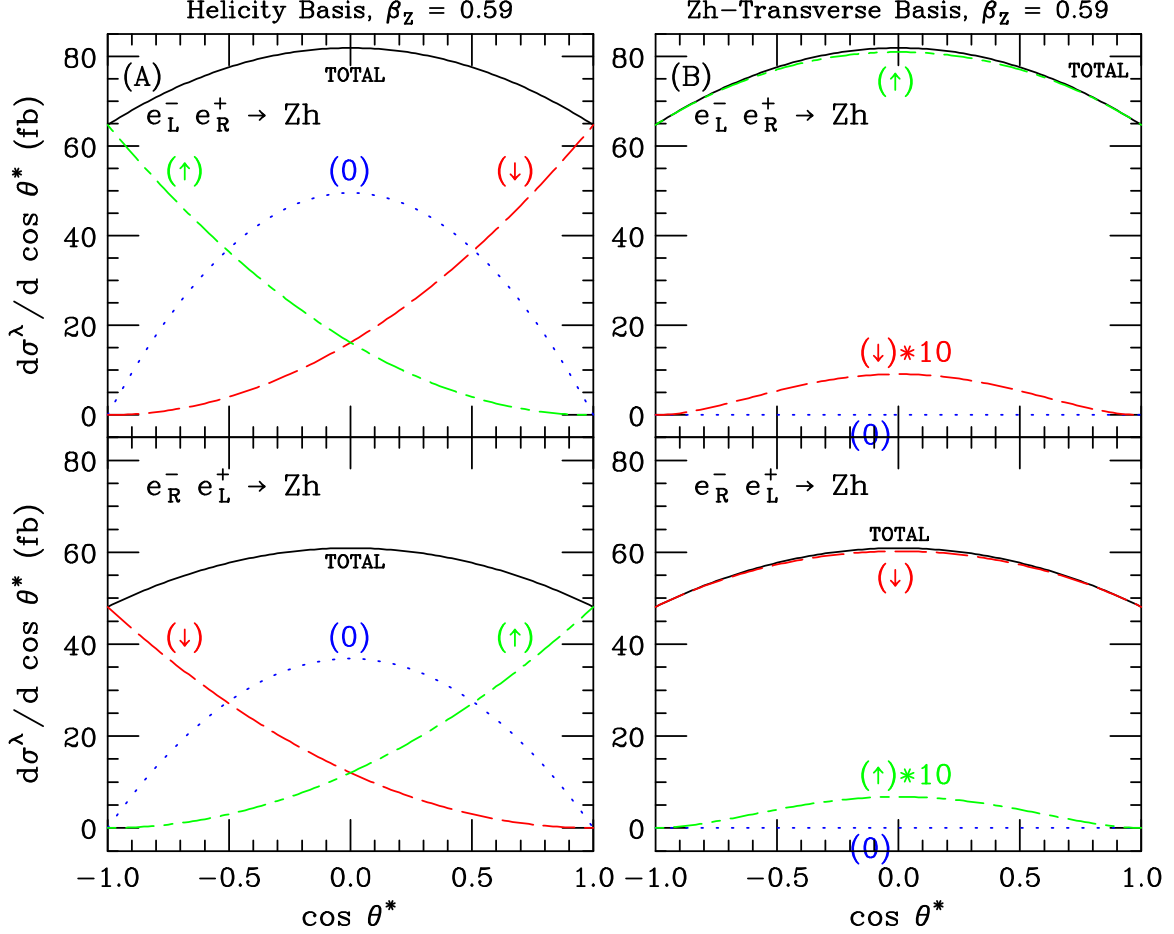


FIG. 4: Production angle distributions for the polarized  $e^+e^- \rightarrow Zh$  cross section assuming  $\sqrt{s} = 250$  GeV and  $M_h = 120$  GeV ( $\beta_z = 0.59$ ). Displayed are the contributions from the three possible  $Z$  spins in **(A)** the helicity basis and **(B)** the  $Zh$ -transverse basis.

By integrating Eq. (17) over  $\cos \theta^*$  we obtain the total cross section for  $e_L^- e_R^+ \rightarrow Zh$ :

$$\sigma_L(e_L^- e_R^+ \rightarrow Zh) = q_{eL}^2 G_F^2 \frac{M_W^2 M_Z^2}{2\pi s} \Theta(s, M_h, M_Z) \left[ 1 - \frac{2}{3} \beta_z^2 \right]. \quad (18)$$

Once again, the result for  $e_R^- e_L^+$  scattering may be generated by the replacement  $q_{eL} \rightarrow q_{eR}$ . Finally, we may divide the differential cross section (17) by the corresponding total cross section to obtain the  $Zh$  production cross section for polarized beams normalized to unity:

$$\begin{aligned} \frac{1}{\sigma_L} \frac{d\sigma_L}{d(\cos \theta^*)} &= \frac{3}{4} \frac{2 - \beta_z^2 (1 + \cos^2 \theta^*)}{3 - 2\beta_z^2} \\ &= \frac{1}{\sigma_R} \frac{d\sigma_R}{d(\cos \theta^*)}. \end{aligned} \quad (19)$$

Eq. (19) explicitly exhibits the fact that the only difference between  $e_L^- e_R^+$  and  $e_R^- e_L^+$  scattering to the  $Zh$  final state is in the overall normalization of the production cross section: the

TABLE II: Spin decompositions in selected bases for  $e^+e^- \rightarrow Zh$  assuming  $m_h = 120$  GeV and  $\sqrt{s} = 250$  GeV ( $\beta_z = 0.59$ ).

	(+)	(-)	(0)
helicity basis:			
$e_L^- e_R^+$	28.3%	28.3%	43.4%
$e_R^- e_L^+$	28.3%	28.3%	43.4%
$e^- e^+$ (unpolarized)	28.3%	28.3%	43.4%
$Zh$ -transverse basis:			
$e_L^- e_R^+$	99.3%	0.7%	0.0% <sup>a</sup>
$e_R^- e_L^+$	0.7%	99.3%	0.0% <sup>a</sup>
$e^- e^+$ (unpolarized)	57.3%	42.7%	0.0% <sup>a</sup>

<sup>a</sup>This contribution is exactly zero (by construction).

shapes of the two distributions are identical. Put another way, the differential cross-section for  $e_R^- e_L^+ \rightarrow Zh$  may be obtained by rescaling the cross section for  $e_L^- e_R^+ \rightarrow Zh$  by the factor  $q_{eR}^2/q_{eL}^2 = 0.7397$ .

## B. Polarized $ZA$ Production

In the Standard Model, the minimal Higgs sector consists of a single complex doublet before spontaneous-symmetry breaking, leading to a physical spectrum that contains only a  $CP$ -even Higgs boson. In extensions to the Standard Model, the Higgs sector is often more complicated, leading to additional physical Higgs states with various quantum numbers. One alternative which occurs frequently is the so-called pseudoscalar Higgs boson  $A^0$  (strictly-speaking, the  $A^0$  is a  $CP$ -odd Higgs; its  $\mathcal{J}^{PC}$  assignment is  $0^{+-}$ ). For example, the minimal supersymmetric standard model (MSSM) contains such a state in addition to a pair of  $0^{++}$  states  $h^0$  and  $H^0$ . Thus, it is interesting to consider how the angular distributions are different for a pseudoscalar Higgs boson.

In order to couple a  $CP$ -odd Higgs boson to a pair of vector bosons in a gauge-invariant

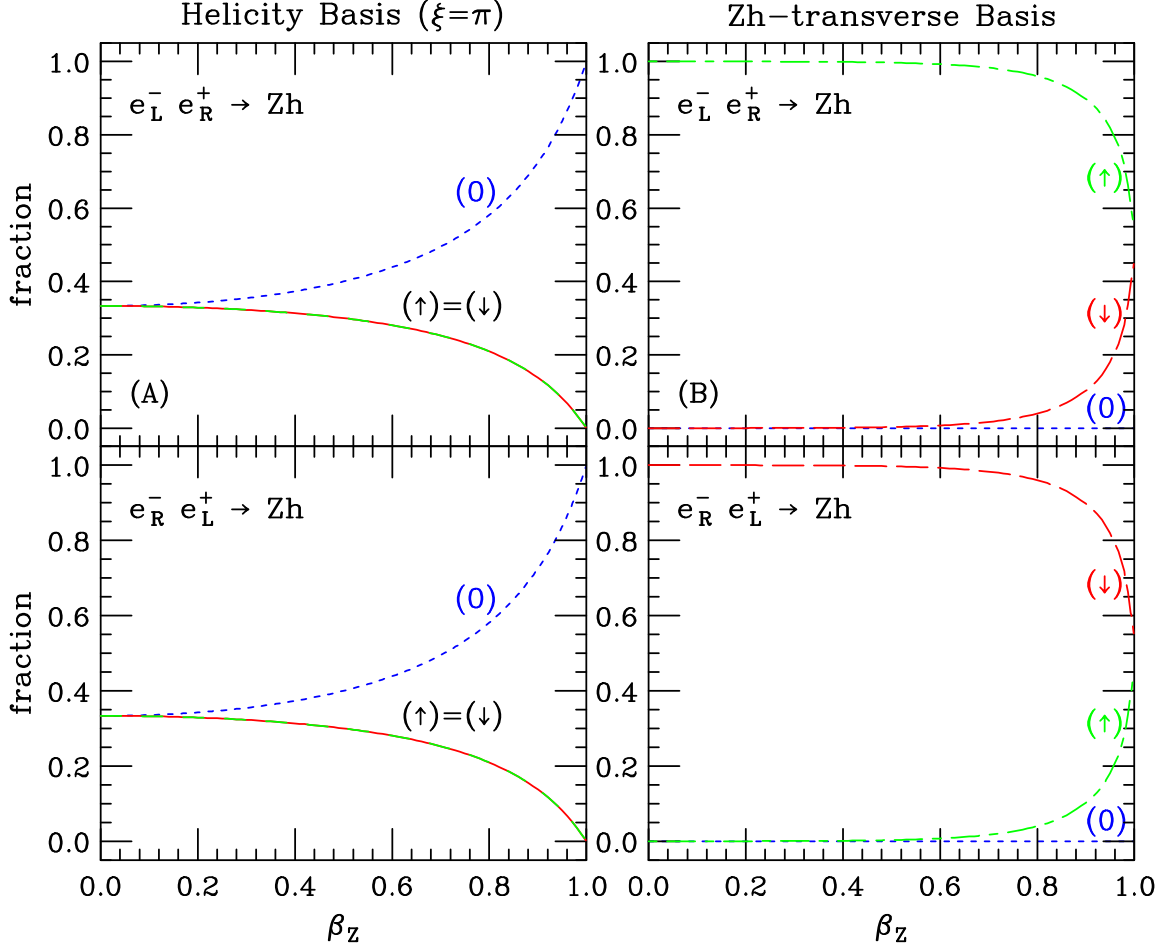


FIG. 5: Spin decomposition in the **(A)** helicity and **(B)**  $Zh$ -transverse bases of the  $e_L^- e_R^+ \rightarrow Zh$  and  $e_R^- e_L^+ \rightarrow Zh$  cross sections as a function of the ZMF speed  $\beta_z$  of the  $Z$  boson. Shown are the fractions of the total cross section in the  $(\uparrow)$ ,  $(\downarrow)$ , and  $(0)$  spin states.

manner that conserves  $CP$ , it is necessary for the interaction to take the form [13]

$$\epsilon_{\mu\nu\rho\sigma} F^{\mu\nu} F^{\rho\sigma} A^0. \quad (20)$$

This is a dimension-5 operator; it cannot appear in the tree-level Lagrangian. Such a coupling can be generated at loop level, however. Thus, as in Ref. [2], we write the (effective)  $ZZA$  vertex as

$$-\frac{igM_Z}{\cos\theta_W} \frac{\eta}{\Lambda^2} k_1^\mu k_2^\nu \epsilon_{\mu\nu\alpha\beta}, \quad (21)$$

where  $k_1$  and  $k_2$  are the 4-momenta of the two  $Z$ 's,  $\eta$  is a dimensionless coupling constant, and  $\Lambda$  is the mass scale at which this vertex is generated [14]. Because of the generality of the argument leading to the form of the coupling in Eqs. (20) and (21), the angular correlations

in a wide variety of models will have this form even though we cannot say very much about the over-all size of the total cross section. Nevertheless, we expect  $e^+e^- \rightarrow Zh$  (if not kinematically suppressed) to dominate over  $e^+e^- \rightarrow ZA$  on the grounds that the one-loop effective  $ZZA$  coupling will likely be smaller than the tree-level  $ZZh$  coupling.

The vertex in Eq. (21) leads to the differential cross sections

$$\frac{d\sigma^\lambda(e_L^-e_R^+\rightarrow ZA)}{d(\cos\theta^*)} = G_F^2 M_W^2 \eta^2 \frac{M_Z^4}{\Lambda^4} \frac{\beta_Z^2}{\pi} \Theta(s, M_A, M_Z) q_{eL}^2 \left[ \tilde{\mathcal{S}}_L^\lambda(\theta^*, \xi) \right]^2 \quad (22)$$

and

$$\frac{d\sigma^\lambda(e_R^-e_L^+\rightarrow ZA)}{d(\cos\theta^*)} = G_F^2 M_W^2 \eta^2 \frac{M_Z^4}{\Lambda^4} \frac{\beta_Z^2}{\pi} \Theta(s, M_A, M_Z) q_{eR}^2 \left[ \tilde{\mathcal{S}}_R^\lambda(\theta^*, \xi) \right]^2 \quad (23)$$

In this case, the spin functions turn out to be independent of energy:

$$\begin{aligned} \tilde{\mathcal{S}}_L^\pm(\theta^*, \xi) &= \frac{1}{\sqrt{2}}(c_\theta \pm c_\xi); \\ \tilde{\mathcal{S}}_L^0(\theta^*, \xi) &= s_\xi. \end{aligned} \quad (24)$$

The spin functions for  $e_R^-e_L^+$  scattering are related to those for  $e_L^-e_R^+$  in the usual fashion, namely

$$\begin{aligned} \tilde{\mathcal{S}}_R^\pm(\theta^*, \xi) &= \tilde{\mathcal{S}}_L^\mp(\theta^*, \xi); \\ \tilde{\mathcal{S}}_R^0(\theta^*, \xi) &= \tilde{\mathcal{S}}_L^0(\theta^*, \xi). \end{aligned} \quad (25)$$

It is obvious from the especially simple form of the spin functions in Eqs. (24) and (25) that the optimal basis for studying angular correlations in  $ZA$  production and decay is the helicity basis, independent of the machine energy. In the helicity basis, the spin functions become

$$\begin{aligned} \tilde{\mathcal{S}}_L^\pm(\theta^*, \pi) &= \frac{1}{\sqrt{2}}(c_\theta \mp 1); \\ \tilde{\mathcal{S}}_L^0(\theta^*, \pi) &= 0. \end{aligned} \quad (26)$$

Only the helicity basis has the property that one of the three amplitudes (the longitudinal one) vanishes.

TABLE III: Spin decompositions in selected bases for  $e^+e^- \rightarrow ZA$  assuming  $m_h = 120$  GeV and  $\sqrt{s} = 250$  GeV ( $\beta_z = 0.59$ ).

	(+)	(-)	(0)
helicity basis:			
$e_L^- e_R^+$	50.0%	50.0%	0.0%
$e_R^- e_L^+$	50.0%	50.0%	0.0%
$e^- e^+$ (unpolarized)	50.0%	50.0%	0.0%
$Zh$ -transverse basis:			
$e_L^- e_R^+$	45.7%	0.1%	54.1%
$e_R^- e_L^+$	0.1%	45.7%	54.1%
$e^- e^+$ (unpolarized)	26.3%	19.6%	54.1%

For the sake of comparison, it is useful to write out the  $ZA$  spin functions in the  $Zh$ -transverse basis:

$$\begin{aligned}
\tilde{\mathcal{S}}_L^\pm(\theta^*, \tan^{-1}(\gamma_z \tan \theta^*)) &= \frac{c_\theta}{\sqrt{2}} \frac{\sqrt{1 - \beta_z^2 c_\theta^2} \pm \sqrt{1 - \beta_z^2}}{\sqrt{1 - \beta_z^2 c_\theta^2}}; \\
\tilde{\mathcal{S}}_L^0(\theta^*, \tan^{-1}(\gamma_z \tan \theta^*)) &= \frac{s_\theta}{\sqrt{1 - \beta_z^2 c_\theta^2}}.
\end{aligned} \tag{27}$$

The results are not particularly simple since this choice of  $\xi$  was concocted to simplify the  $Zh$  amplitudes, not the  $ZA$  amplitudes. We display the  $\cos \theta^*$ -dependence of these contributions to the  $ZA$  production cross section in Fig. 6 for the same Higgs mass and machine energy as previously. Perhaps surprisingly, one of the spin states is highly suppressed in the  $Zh$ -transverse basis when we use polarized beams. This is in contrast to the helicity basis, where the  $(\uparrow)$  and  $(\downarrow)$  states provide equal contributions to the total cross section.

In Fig. 7 we plot the  $Z$  spin decomposition in  $e^+e^- \rightarrow ZA$  production as a function of  $\beta_z$ . Table III lists selected numerical values for this spin breakdown. A consequence of the energy-independence of the spin functions contained in Eqs. (24) and (25) is that all of the  $\beta_z$ -dependence exhibited in these plots comes from choosing  $\xi$  to be an explicit function of  $\beta_z$ . In the helicity basis, the spin breakdown is 50-50 between the  $(\uparrow)$  and  $(\downarrow)$  spin states for all center-of-mass energies. On the other hand, in the (non-optimal for  $ZA$  production)  $Zh$ -transverse basis, we have a 50-50 mix of the (0) and  $(\uparrow)$  or (0) and  $(\downarrow)$  spin



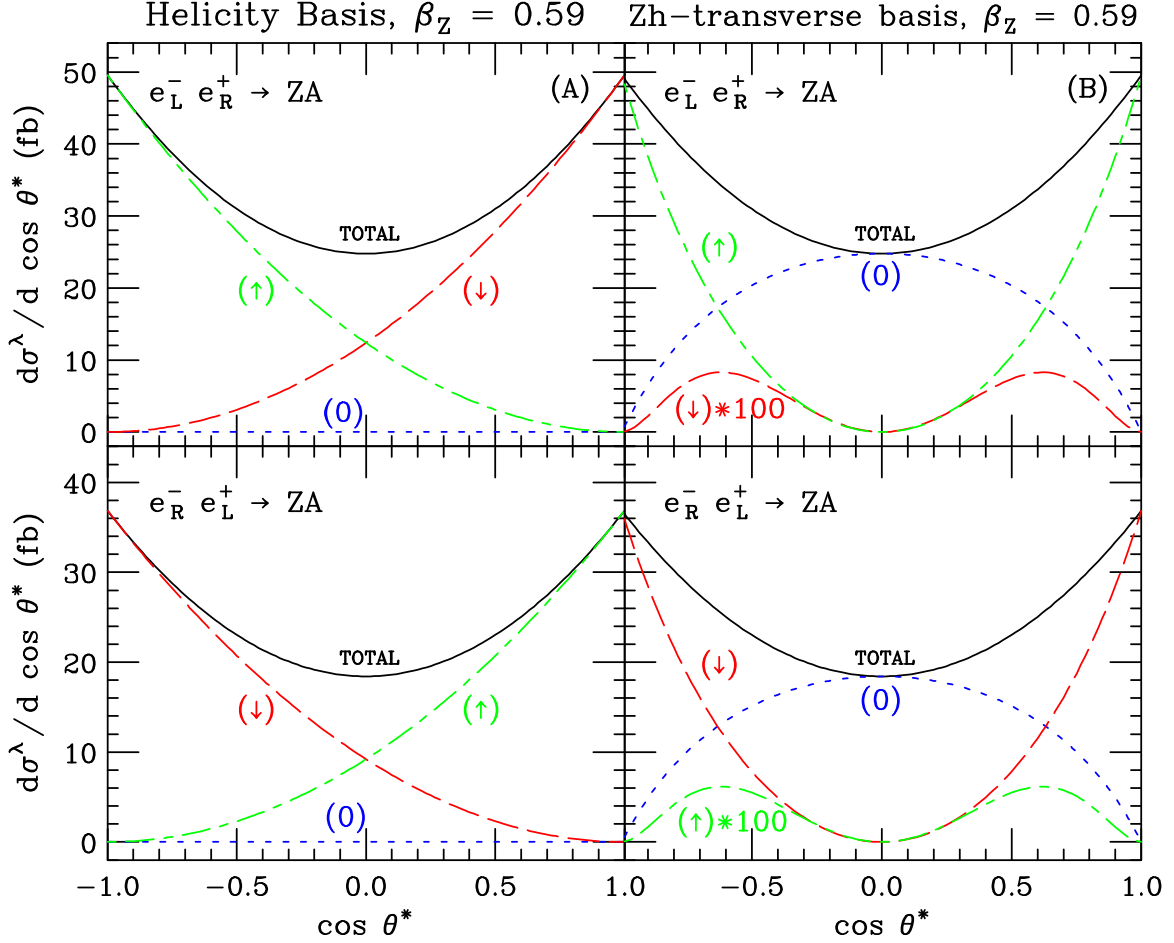


FIG. 6: Production angle distributions for the polarized  $e^+e^- \rightarrow ZA$  cross section assuming  $\sqrt{s} = 250$  GeV and  $M_h = 120$  GeV ( $\beta_z = 0.59$ ) broken down into the contributions from the three possible  $Z$  spins, in the **(A)** helicity and **(B)**  $Zh$ -transverse bases.

states near threshold, with the fraction of longitudinal  $Z$ 's gradually increasing as  $\beta_z \rightarrow 1$ . Thus, we are left with the linguistically-awkward situation where in the  $Zh$ -transverse basis,  $ZA$  production is dominated by the *longitudinal* component!

Summing over the possible spins of the  $Z$  we find that the total differential cross section corresponding to the spin functions in Eq. (24) reads

$$\sum_{\lambda} \frac{d\sigma_L^{\lambda}}{d(\cos \theta^*)} = q_{eL}^2 G_F^2 M_W^2 \eta^2 \frac{M_Z^4}{\Lambda^4} \frac{\beta_z^2}{\pi} \Theta(s, M_A, M_Z) (1 + \cos^2 \theta^*). \quad (28)$$

The corresponding result for  $e_R^- e_L^+$  scattering differs only by the replacement  $q_{eL}^2 \rightarrow q_{eR}^2$ . Integrating over  $\cos \theta^*$  gives the total polarized  $ZA$  production cross section

$$\sigma_L(e^+e^- \rightarrow ZA) = \frac{8}{3} q_{eL}^2 G_F^2 M_W^2 \eta^2 \frac{M_Z^4}{\Lambda^4} \frac{\beta_z^2}{\pi} \Theta(s, M_A, M_Z). \quad (29)$$

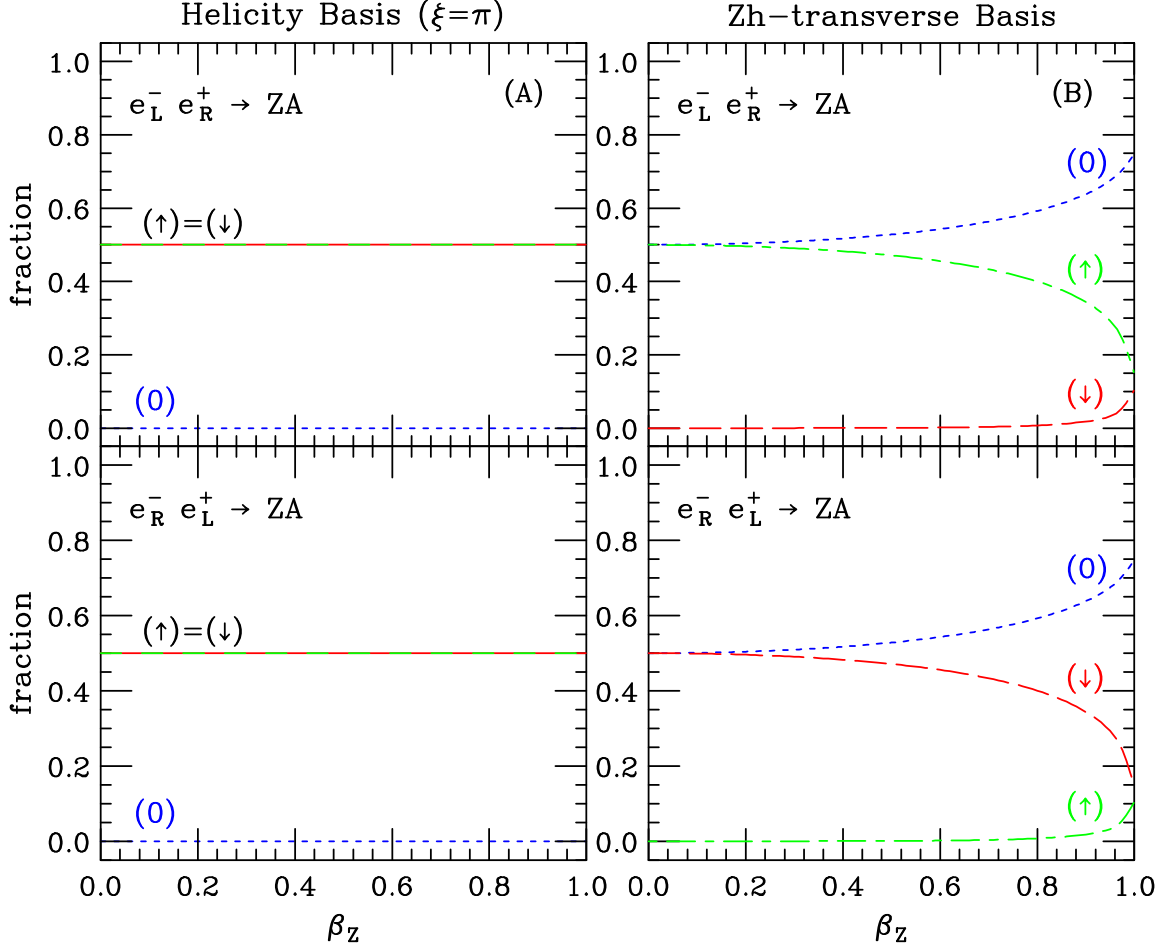


FIG. 7: Spin decomposition in the **(A)** helicity and **(B)**  $Zh$ -transverse bases of the  $e_L^- e_R^+ \rightarrow ZA$  and  $e_R^- e_L^+ \rightarrow ZA$  cross sections as a function of the ZMF speed  $\beta_z$  of the  $Z$  boson. Shown are the fractions of the total cross section in the  $(\uparrow)$ ,  $(\downarrow)$ , and  $(0)$  spin states.

The result for  $\sigma_R(e^+ e^- \rightarrow ZA)$  follows from Eq. (29) by the replacement  $q_{eL}^2 \rightarrow q_{eR}^2$ . Thus, the normalized differential distributions are

$$\begin{aligned} \frac{1}{\sigma_L} \frac{d\sigma_L}{d(\cos \theta^*)} &= \frac{3}{8} (1 + \cos^2 \theta^*) \\ &= \frac{1}{\sigma_R} \frac{d\sigma_R}{d(\cos \theta^*)}. \end{aligned} \quad (30)$$

#### IV. POLARIZED $Z$ DECAYS

The  $Zf\bar{f}$  coupling violates both parity and flavor universality. Thus, the angular distributions for the decay of polarized  $Z$  bosons are forward-backward asymmetric, and depend on which fermions appear in the final state. Neglecting the mass of the final state fermions [15], the angular distributions in the rest frame of the decaying  $Z$  may be written as

$$\frac{1}{\Gamma_f} \frac{d\Gamma^\lambda}{d(\cos \chi)} = \frac{3}{8} \left\{ \frac{q_{fL}^2}{q_{fL}^2 + q_{fR}^2} |\mathfrak{D}_L^\lambda|^2 + \frac{q_{fR}^2}{q_{fL}^2 + q_{fR}^2} |\mathfrak{D}_R^\lambda|^2 \right\}. \quad (31)$$

In these expressions, the decay of the  $Z$  boson in spin state  $\lambda$  to  $f_L\bar{f}_R$  is described by the amplitudes

$$\begin{aligned} \mathfrak{D}_L^\pm &\equiv e^{\pm i\varphi} (c_\chi \pm 1), \\ \mathfrak{D}_L^0 &\equiv s_\chi \sqrt{2}, \end{aligned} \quad (32)$$

whereas the decay to a  $f_R\bar{f}_L$  final state depends on

$$\begin{aligned} \mathfrak{D}_R^\pm &= \mathfrak{D}_L^{\mp*}, \\ \mathfrak{D}_R^0 &= \mathfrak{D}_L^{0*}. \end{aligned} \quad (33)$$

These distributions have been normalized to unit area by inclusion of the partial width  $\Gamma_f$  for the decay  $Z \rightarrow f\bar{f}$ . We define  $\chi$  to be the angle between the direction of motion of the fermion and the spin axis as seen in the  $Z$  rest frame. The distributions represented by Eq. (31) can also be written in the form

$$\frac{1}{\Gamma_f} \frac{d\Gamma^\pm}{d(\cos \chi)} = \frac{3}{8} \left[ (1 + \cos^2 \chi) \pm 2 \frac{q_{fL}^2 - q_{fR}^2}{q_{fL}^2 + q_{fR}^2} \cos \chi \right] \quad (34)$$

for the transverse polarizations and

$$\frac{1}{\Gamma_f} \frac{d\Gamma^0}{d(\cos \chi)} = \frac{3}{4} \sin^2 \chi \quad (35)$$

for the longitudinal state. For convenience, we have collected the Standard Model values of the combination of coupling constants appearing in the  $\cos \chi$  term of Eq. (34) in Table IV. The corresponding distributions are plotted in Fig. 8. Unfortunately, the decays with the most distinctive distributions,  $Z \rightarrow \nu\bar{\nu}$ , are invisible. On the other hand, for the decays for which charge/flavor identification would be the easiest,  $Z \rightarrow \ell\bar{\ell}$ , we have a fairly large overlap between the  $(\uparrow)$  and  $(\downarrow)$  distributions. Although the charge and flavor identification

TABLE IV: Coefficients for  $Z$  decay. The numerical values correspond to  $\sin^2 \theta_W = 0.2312$ . The final entry is for a jet of undetermined charge.

fermion	$\frac{q_{fL}^2 - q_{fR}^2}{q_{fL}^2 + q_{fR}^2}$		value
$u, c$	$\frac{9 - 24 \sin^2 \theta_W}{9 - 24 \sin^2 \theta_W + 32 \sin^4 \theta_W}$	=	0.6686
$d, s, b$	$\frac{9 - 12 \sin^2 \theta_W}{9 - 12 \sin^2 \theta_W + 8 \sin^4 \theta_W}$	=	0.9387
$e, \mu, \tau$	$\frac{1 - 4 \sin^2 \theta_W}{1 - 4 \sin^2 \theta_W + 8 \sin^4 \theta_W}$	=	0.1496
$\nu$	1	=	1.0000
$q/\bar{q}$ (unspecified)	0	=	0.0000

for decays to light quarks is virtually impossible, there is some efficiency for distinguishing  $b$  from  $\bar{b}$ . Therefore, we will highlight this  $Z$  decay mode when illustrating our results. Even if it turns out to be too optimistic to distinguish  $b$ -jets from  $\bar{b}$ -jets, it will still be possible to do  $Zh/Z\bar{A}$  differentiation because, as we will see shortly, simply separating the longitudinal and transverse polarization states should be sufficient to provide interesting information about the nature of the associated Higgs boson.

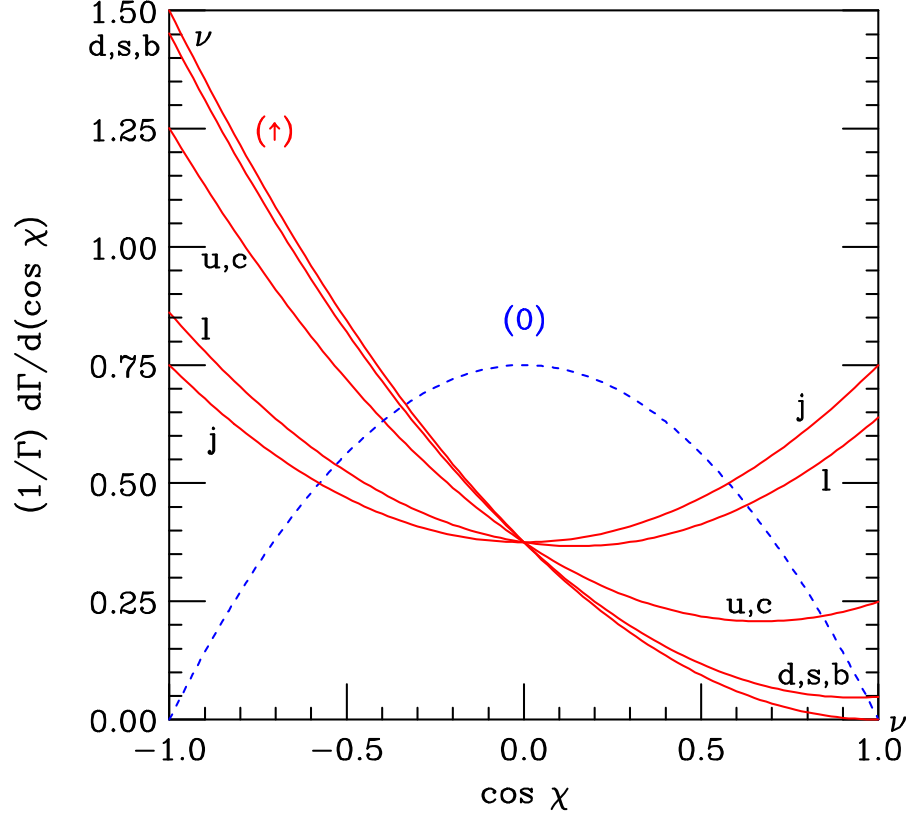


FIG. 8: Angular distributions for the decay of a polarized  $Z$ , spin state  $(\uparrow)$  (solid curves) or  $(0)$  (dashed curve).  $\chi$  is the angle between the direction of the fermion ( $\nu, l, u, d, s, c$  or  $b$ ) and the chosen spin axis, as viewed in the  $Z$  rest frame. The decay distribution for a transversely-polarized  $Z$  boson depends on the flavor of the decay product as labeled; the decay of a longitudinally-polarized  $Z$  does not.  $l$  is a generic charged lepton and may be any of  $e^-$ ,  $\mu^-$ , or  $\tau^-$ ;  $j$  is a quark or antiquark jet of any flavor. The distributions for the decay of a  $Z$  in the  $(\downarrow)$  spin state may be generated by replacing  $\cos \chi \rightarrow -\cos \chi$  in the  $(\uparrow)$  distribution.

## V. PRODUCTION AND DECAY COMBINED

### A. $Zh$ case

The complete cross section for the production and decay of a  $Z$  and a Higgs may be written and understood in terms of the cross section for the production of a  $Z$  boson with spin  $\lambda$  [Eqs. (3) and (4)] multiplied by amplitudes describing its decay [Eqs. (32) and (33)]. We define the following angles to describe the process:  $\theta^*$  refers to the  $Z$  boson production angle as seen in the ZMF;  $\chi$  is the angle between the direction of motion of the fermion (*i.e.*

the spatial part of the 4-vector  $f$ ) and the spin axis as seen in the  $Z$  rest frame; and  $\varphi$  is the azimuthal angle associated with this decay (*i.e.* the angle between the  $Zh$  production plane and the  $Z$  decay plane), also viewed in the  $Z$  rest frame. With these definitions, the triply-differential cross sections for  $e^+e^- \rightarrow Zh \rightarrow f\bar{f}h$  read

$$\begin{aligned} \frac{d^3\sigma_L}{d(\cos\theta^*)d(\cos\chi)d\varphi} &= \frac{3q_{eL}^2}{1024\pi^3} \frac{M_Z^3}{s\Gamma_Z} G_F^2 M_W^2 \Theta(s, M_h, M_Z) \\ &\times \left\{ q_{fL}^2 \left| \mathfrak{D}_L^+ \mathcal{S}_L^+ + \mathfrak{D}_L^0 \mathcal{S}_L^0 + \mathfrak{D}_L^- \mathcal{S}_L^- \right|^2 \right. \\ &\quad \left. + q_{fR}^2 \left| \mathfrak{D}_R^+ \mathcal{S}_L^+ + \mathfrak{D}_R^0 \mathcal{S}_L^0 + \mathfrak{D}_R^- \mathcal{S}_L^- \right|^2 \right\} \end{aligned} \quad (36)$$

and

$$\begin{aligned} \frac{d^3\sigma_R}{d(\cos\theta^*)d(\cos\chi)d\varphi} &= \frac{3q_{eR}^2}{1024\pi^3} \frac{M_Z^3}{s\Gamma_Z} G_F^2 M_W^2 \Theta(s, M_h, M_Z) \\ &\times \left\{ q_{fL}^2 \left| \mathfrak{D}_L^+ \mathcal{S}_R^+ + \mathfrak{D}_L^0 \mathcal{S}_R^0 + \mathfrak{D}_L^- \mathcal{S}_R^- \right|^2 \right. \\ &\quad \left. + q_{fR}^2 \left| \mathfrak{D}_R^+ \mathcal{S}_R^+ + \mathfrak{D}_R^0 \mathcal{S}_R^0 + \mathfrak{D}_R^- \mathcal{S}_R^- \right|^2 \right\}. \end{aligned} \quad (37)$$

Since the gamut of potentially interesting spin bases does not extend to those with dependence on the azimuthal angle, we may deal with  $\varphi$  once and for all by inserting the expressions for the decay amplitudes contained in Eqs. (32) and (33) into Eq. (36), performing the azimuthal integration, and doing a bit of rearrangement to arrive at

$$\begin{aligned} \frac{d^2\sigma_L}{dc_\theta dc_\chi} &= \frac{3q_{eL}^2}{512\pi^3} (q_{fL}^2 + q_{fR}^2) \frac{M_Z^3}{s\Gamma_Z} G_F^2 M_W^2 \Theta(s, M_h, M_Z) \\ &\times \left\{ (1 + c_\chi^2) |\mathcal{M}^+|^2 + 2s_\chi^2 |\mathcal{M}^0|^2 + (1 + c_\chi^2) |\mathcal{M}^-|^2 \right. \\ &\quad \left. + \frac{q_{fL}^2 - q_{fR}^2}{q_{fL}^2 + q_{fR}^2} (2\cos\chi) [|\mathcal{M}^+|^2 - |\mathcal{M}^-|^2] \right\}, \end{aligned} \quad (38)$$

where we have defined

$$\mathcal{M}^+ \equiv \mathcal{S}_L^+ = \mathcal{S}_R^-; \quad \mathcal{M}^- \equiv \mathcal{S}_L^- = \mathcal{S}_R^+; \quad \mathcal{M}^0 \equiv \mathcal{S}_L^0 = \mathcal{S}_R^0. \quad (39)$$

Substitution of the explicit forms of the spin functions in the  $Zh$ -transverse basis from Eq. (16) allows us to write the cross section in Eq. (38) in the relatively simple form

$$\begin{aligned} \left. \frac{d^2\sigma_L}{dc_\theta dc_\chi} \right|_{\text{trans}} &= \frac{3q_{eL}^2}{512\pi^3} (q_{fL}^2 + q_{fR}^2) \frac{M_Z^3}{s\Gamma_Z} G_F^2 M_W^2 \Theta(s, M_h, M_Z) \\ &\times \left\{ (1 + c_\chi^2) [2 - \beta_Z^2 (1 + c_\theta^2)] \right\} \end{aligned}$$

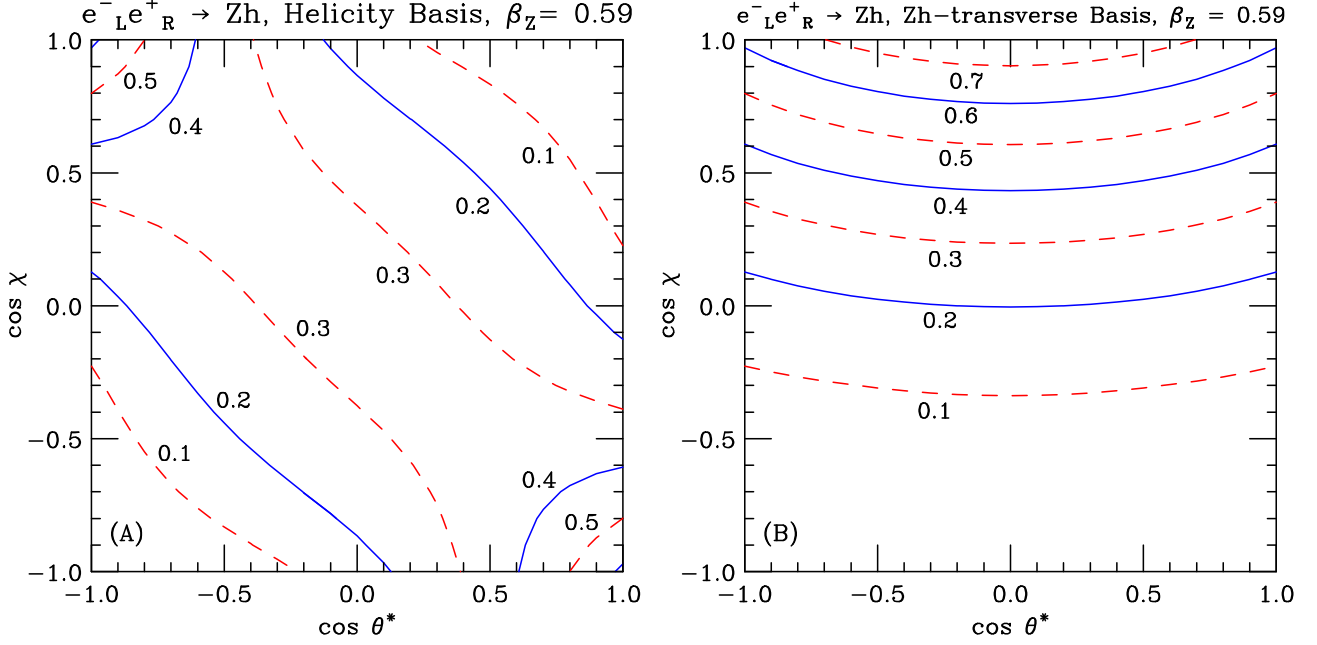


FIG. 9: Double differential production and decay distributions for  $e^+e^- \rightarrow Zh \rightarrow b\bar{b}h$ , normalized to unity, assuming  $\sqrt{s} = 250$  GeV and  $M_h = 120$  GeV ( $\beta_z = 0.59$ ). Shown are the results using (A) the helicity basis and (B) the  $Zh$ -transverse basis.

$$+ \frac{q_{fL}^2 - q_{fR}^2}{q_{fL}^2 + q_{fR}^2} (2 \cos \chi) \left[ 2\gamma_z^{-1} \sqrt{1 - \beta_z^2 c_\theta^2} \right] \Big\}. \quad (40)$$

Using the helicity basis instead leads to a slightly more complicated result:

$$\begin{aligned} \left. \frac{d^2 \sigma_L}{dc_\theta dc_\chi} \right|_{\text{helicity}} &= \frac{3q_{eL}^2}{512\pi^3} (q_{fL}^2 + q_{fR}^2) \frac{M_z^3}{s\Gamma_z} G_F^2 M_W^2 \Theta(s, M_h, M_z) \\ &\times \left\{ (1 - \beta_z^2)(1 + c_\chi^2)(1 + c_\theta^2) + 2s_\chi^2 s_\theta^2 \right. \\ &\quad \left. - 4\gamma_z^{-1} \frac{q_{fL}^2 - q_{fR}^2}{q_{fL}^2 + q_{fR}^2} \cos \chi \cos \theta^* \right\}. \end{aligned} \quad (41)$$

The distributions contained in Eqs. (40) and (41) have been plotted in Fig. 9 at  $\beta_z = 0.59$ : that is, for a Higgs mass of 120 GeV and a collider center-of-mass energy of 250 GeV.

The analogous procedure applied to Eq. (37) leads to a similar result which may be generated from Eq. (38) by the interchanges  $q_{eL} \leftrightarrow q_{eR}$ ;  $q_{fL} \leftrightarrow q_{fR}$ . Performing the average over the initial spins leads to the unpolarized result

$$\begin{aligned} \frac{d^2 \sigma_U}{dc_\theta dc_\chi} &= \frac{3}{2048\pi^3} (q_{eL}^2 + q_{eR}^2)(q_{fL}^2 + q_{fR}^2) \frac{M_z^3}{s\Gamma_z} G_F^2 M_W^2 \Theta(s, M_h, M_z) \\ &\times \left\{ (1 + c_\chi^2) |\mathcal{M}^+|^2 + 2s_\chi^2 |\mathcal{M}^0|^2 + (1 + c_\chi^2) |\mathcal{M}^-|^2 \right\} \end{aligned}$$

$$+ \frac{q_{eL}^2 - q_{eR}^2}{q_{eL}^2 + q_{eR}^2} \frac{q_{fL}^2 - q_{fR}^2}{q_{fL}^2 + q_{fR}^2} (2 \cos \chi) \left[ |\mathcal{M}^+|^2 - |\mathcal{M}^-|^2 \right] \Big\}. \quad (42)$$

The differences in the shapes of the polarized and unpolarized distributions are completely contained in the forward-backward asymmetric ( $\cos \chi$ ) term, the coefficient of which depends on the difference between the left and right hand fermion-to- $Z$  couplings as well as the flavor of fermion involved. It should be clear from this discussion plus the similarities between Eqs. (38) and (42) that it is not necessary to perform the full calculation separately for each of the three cases: knowledge of just one case plus suitable alteration of the coefficient of the  $\cos \chi$  term is sufficient to generate the other two distributions. For polarized beams the asymmetry factor depends only on the nature of the  $Z$  decay products, whereas if the beams are unpolarized, an additional factor involving the electron-to- $Z$  couplings dilutes the forward-backward asymmetry. A glance at Table IV reveals that this dilution factor is rather small, only about 0.15; therefore, the observation of forward-backward asymmetries will be greatly aided by the use of polarized beams.

By choosing a slightly different rearrangement/grouping of the terms in Eq. (38) and incorporating the information on the shape of the polarized  $Z$  decay distributions contained in Eqs. (34) and (35), we conclude that the fraction of  $Z$ 's produced in spin state  $\lambda$  from  $e_L^- e_R^+$  scattering may be calculated from

$$f_L^\lambda = \frac{\int_{-1}^1 dc_\theta |\mathcal{S}_L^\lambda|^2}{\int_{-1}^1 dc_\theta \left\{ |\mathcal{S}_L^+|^2 + |\mathcal{S}_L^0|^2 + |\mathcal{S}_L^-|^2 \right\}}. \quad (43)$$

For  $e_R^- e_L^+$  scattering, we should replace the  $\mathcal{S}_L$ 's with  $\mathcal{S}_R$ 's in the above formula; for unpolarized beams, we should form the appropriate weighted average of the left-handed and right-handed fractions:

$$f_U^\lambda = \frac{q_{eL}^2}{q_{eL}^2 + q_{eR}^2} f_L^\lambda + \frac{q_{eR}^2}{q_{eL}^2 + q_{eR}^2} f_R^\lambda \quad (44)$$

Eqs. (43) and (44) may be used to determine the spin fractions using any spin basis in any model for which the polarized production amplitudes  $\mathcal{S}_{L,R}^\lambda$  have been calculated.

## B. $ZA$ case

We now turn to the analogous treatment for the case of a  $CP$ -odd boson. We begin by writing the the triply-differential cross-section for the production and decay process



$e_L^- e_R^+ \rightarrow ZA \rightarrow f\bar{f}A$  in terms of the previously-defined production [Eqs. (24) and (25)] and decay [Eqs. (32) and (33)] amplitudes:

$$\begin{aligned} \frac{d^3\sigma_L}{d(\cos\theta^*)d(\cos\chi)d\varphi} &= \frac{3\beta_z^2}{128\pi^3} \frac{M_z}{\Gamma_z} \eta^2 \frac{M_z^4}{\Lambda^4} q_{eL}^2 G_F^2 M_W^2 \Theta(s, M_A, M_z) \\ &\times \left\{ q_{fL}^2 \left| \mathfrak{D}_L^+ \tilde{\mathcal{S}}_L^+ + \mathfrak{D}_L^0 \tilde{\mathcal{S}}_L^0 + \mathfrak{D}_L^- \tilde{\mathcal{S}}_L^- \right|^2 \right. \\ &\quad \left. + q_{fR}^2 \left| \mathfrak{D}_R^+ \tilde{\mathcal{S}}_L^+ + \mathfrak{D}_R^0 \tilde{\mathcal{S}}_L^0 + \mathfrak{D}_R^- \tilde{\mathcal{S}}_L^- \right|^2 \right\}. \end{aligned} \quad (45)$$

As in the  $Zh$  case, we are not interested in spin bases that explicitly depend on  $\varphi$ . Thus, we integrate over  $\varphi$  by inserting the explicit decay amplitudes for the  $Z$  boson and perform a bit of algebra to obtain

$$\begin{aligned} \frac{d^2\sigma_L}{dc_\theta dc_\chi} &= \frac{3\beta_z^2}{64\pi^2} \frac{M_z}{\Gamma_z} \eta^2 \frac{M_z^4}{\Lambda^4} q_{eL}^2 (q_{fL}^2 + q_{fR}^2) G_F^2 M_W^2 \Theta(s, M_A, M_z) \\ &\times \left\{ (1 + c_\chi^2) |\widetilde{\mathcal{M}}^+|^2 + 2s_\chi^2 |\widetilde{\mathcal{M}}^0|^2 + (1 + c_\chi^2) |\widetilde{\mathcal{M}}^-|^2 \right. \\ &\quad \left. + \frac{q_{fL}^2 - q_{fR}^2}{q_{fL}^2 + q_{fR}^2} (2 \cos \chi) \left[ |\widetilde{\mathcal{M}}^+|^2 - |\widetilde{\mathcal{M}}^-|^2 \right] \right\}, \end{aligned} \quad (46)$$

where it is natural to introduce the following definitions:

$$\widetilde{\mathcal{M}}^+ \equiv \tilde{\mathcal{S}}_L^+ = \tilde{\mathcal{S}}_R^-; \quad \widetilde{\mathcal{M}}^- \equiv \tilde{\mathcal{S}}_L^- = \tilde{\mathcal{S}}_R^+; \quad \widetilde{\mathcal{M}}^0 \equiv \tilde{\mathcal{S}}_L^0 = \tilde{\mathcal{S}}_R^0. \quad (47)$$

The explicit result for the cross section contained in Eq. (46) is reasonably simple in the helicity basis:

$$\begin{aligned} \left. \frac{d^2\sigma_L}{dc_\theta dc_\chi} \right|_{\text{helicity}} &= \frac{3\beta_z^2}{64\pi^2} \frac{M_z}{\Gamma_z} \eta^2 \frac{M_z^4}{\Lambda^4} q_{eL}^2 (q_{fL}^2 + q_{fR}^2) G_F^2 M_W^2 \Theta(s, M_A, M_z) \\ &\times \left\{ (1 + c_\chi^2)(1 + c_\theta^2) - 4 \frac{q_{fL}^2 - q_{fR}^2}{q_{fL}^2 + q_{fR}^2} \cos \chi \cos \theta^* \right\}, \end{aligned} \quad (48)$$

On the other hand, using the (“wrong”)  $Zh$ -transverse basis for the spin functions instead yields

$$\begin{aligned} \left. \frac{d^2\sigma_L}{dc_\theta dc_\chi} \right|_{\text{trans}} &= \frac{3\beta_z^2}{64\pi^2} \frac{M_z}{\Gamma_z} \eta^2 \frac{M_z^4}{\Lambda^4} q_{eL}^2 (q_{fL}^2 + q_{fR}^2) G_F^2 M_W^2 \Theta(s, M_A, M_z) \\ &\times \left\{ (1 + c_\chi^2) c_\theta^2 \frac{2 - \beta_z^2(1 + c_\theta^2)}{1 - \beta_z^2 c_\theta^2} + 2 \frac{s_\chi^2 s_\theta^2}{1 - \beta_z^2 c_\theta^2} \right. \\ &\quad \left. + \frac{q_{fL}^2 - q_{fR}^2}{q_{fL}^2 + q_{fR}^2} (4 \cos \chi \cos^2 \theta^*) \frac{\sqrt{1 - \beta_z^2}}{\sqrt{1 - \beta_z^2 c_\theta^2}} \right\}, \end{aligned} \quad (49)$$

These two distributions are compared in Fig. 10.

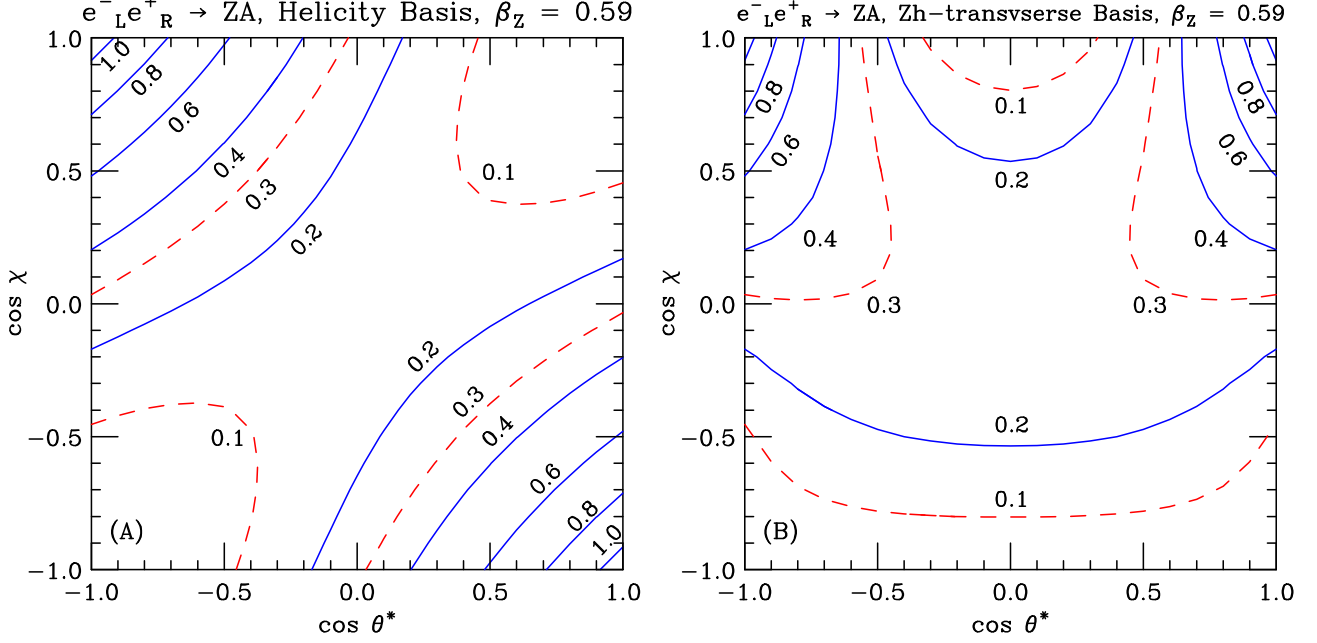


FIG. 10: Double differential production and decay distributions for  $e^+e^- \rightarrow ZA \rightarrow b\bar{b}A$ , normalized to unity, assuming  $\sqrt{s} = 250$  GeV and  $M_h = 120$  GeV ( $\beta_z = 0.59$ ). Shown are the results using (A) the helicity basis and (B) the  $Zh$ -transverse basis.

The result of the corresponding calculation for the  $e_R^- e_L^+$  initial state may be obtained from Eq. (46) by the interchanges  $q_{eL} \leftrightarrow q_{eR}$ ;  $q_{fL} \leftrightarrow q_{fR}$ . Combining the two beam polarizations in the appropriate manner leads to the unpolarized production and decay distribution

$$\begin{aligned} \frac{d^2\sigma_U}{dc_\theta dc_\chi} = & \frac{3\beta_z^2}{256\pi^2} \frac{M_Z}{\Gamma_Z} \eta^2 \frac{M_Z^4}{\Lambda^4} (q_{eL}^2 + q_{eR}^2)(q_{fL}^2 + q_{fR}^2) G_F^2 M_W^2 \Theta(s, M_A, M_Z) \\ & \times \left\{ (1 + c_\chi^2) |\widetilde{\mathcal{M}}^+|^2 + 2s_\chi^2 |\widetilde{\mathcal{M}}^0|^2 + (1 + c_\chi^2) |\widetilde{\mathcal{M}}^-|^2 \right. \\ & \left. + \frac{q_{eL}^2 - q_{eR}^2}{q_{eL}^2 + q_{eR}^2} \frac{q_{fL}^2 - q_{fR}^2}{q_{fL}^2 + q_{fR}^2} (2 \cos \chi) [|\widetilde{\mathcal{M}}^+|^2 - |\widetilde{\mathcal{M}}^-|^2] \right\}. \end{aligned} \quad (50)$$

A careful comparison of Eqs. (46) and (50) reveals that the unpolarized distribution may be obtained from the left-handed distribution by replacing  $q_{eL}^2 \rightarrow \frac{1}{4}(q_{eL}^2 + q_{eR}^2)$  in the prefactor and adjusting the coefficient of the term linear in  $\cos \chi$  as follows:

$$\frac{q_{fL}^2 - q_{fR}^2}{q_{fL}^2 + q_{fR}^2} \rightarrow \frac{q_{eL}^2 - q_{eR}^2}{q_{eL}^2 + q_{eR}^2} \frac{q_{fL}^2 - q_{fR}^2}{q_{fL}^2 + q_{fR}^2}. \quad (51)$$

The fraction of  $Z$  bosons produced in each of the three possible spin states may be calculated from an expression similar to Eqn. (43), but with the  $\mathcal{S}$ 's replaced by  $\widetilde{\mathcal{S}}$ 's.

## VI. $Z$ DECAY ANGULAR DISTRIBUTIONS

At last we come to the decay angular distribution  $d\sigma/d(\cos\chi)$  which will be useful in distinguishing  $Zh$  from  $ZA$ . Since the choice of spin basis influences the exact definition of  $\chi$ , this distribution will depend on the choice made for  $\xi$ . Put differently, the decay angular distribution may be written in the form

$$\frac{1}{\sigma} \frac{d\sigma}{d(\cos\chi)} = f^+ \frac{1}{\Gamma_f} \frac{d\Gamma^+}{d(\cos\chi)} + f^0 \frac{1}{\Gamma_f} \frac{d\Gamma^0}{d(\cos\chi)} + f^- \frac{1}{\Gamma_f} \frac{d\Gamma^-}{d(\cos\chi)}, \quad (52)$$

where the spin fractions may be calculated from Eq. (43) for polarized beams or from Eq. (44) for unpolarized beams. The unit-normalized  $Z$  decay distributions are given by Eqs. (34) and (35). That is, the decay angular distribution is simply a linear superposition of the polarized  $Z$  decay distributions weighted by the fraction of  $Z$ 's in each spin state. Clearly the fraction of  $Z$ 's with a given spin depends on the choice of spin axis. The decay distribution  $d\sigma/d(\cos\chi)$  in a particular spin basis may be calculated by inserting the desired expressions for  $s_\xi$  and  $c_\xi$  into the spin functions (9) and (10), and then using the results to calculate the spin fractions from Eq. (43).

### A. $Zh$ in the helicity basis

For example, setting  $\xi = \pi$  to obtain the helicity basis leads to

$$\left. \frac{1}{\sigma_L} \frac{d\sigma_L}{d(\cos\chi)} \right|_{\text{helicity}} = \frac{3}{12 - 8\beta_z^2} \left[ 2 - \beta_z^2 (1 + \cos^2\chi) \right]. \quad (53)$$

In the panels on the left-hand side of Fig. 11 we have plotted this distribution for  $\beta_z = 0.5$  and 0.9. The distribution is nearly flat in  $\cos\chi$  close to threshold ( $\beta_z = 0$ ), and becomes more and more concave down as  $\beta_z$  is increased. For  $\beta_z \rightarrow 1$  (the ultra-relativistic limit) we have

$$\left. \frac{1}{\sigma_T} \frac{d\sigma}{d(\cos\chi)} \right|_{\text{helicity}} \longrightarrow \frac{3}{4} \sin^2\chi, \quad (54)$$

the signature of  $Z$  bosons produced with 100% longitudinal polarization in accordance with the vector boson equivalence theorem.

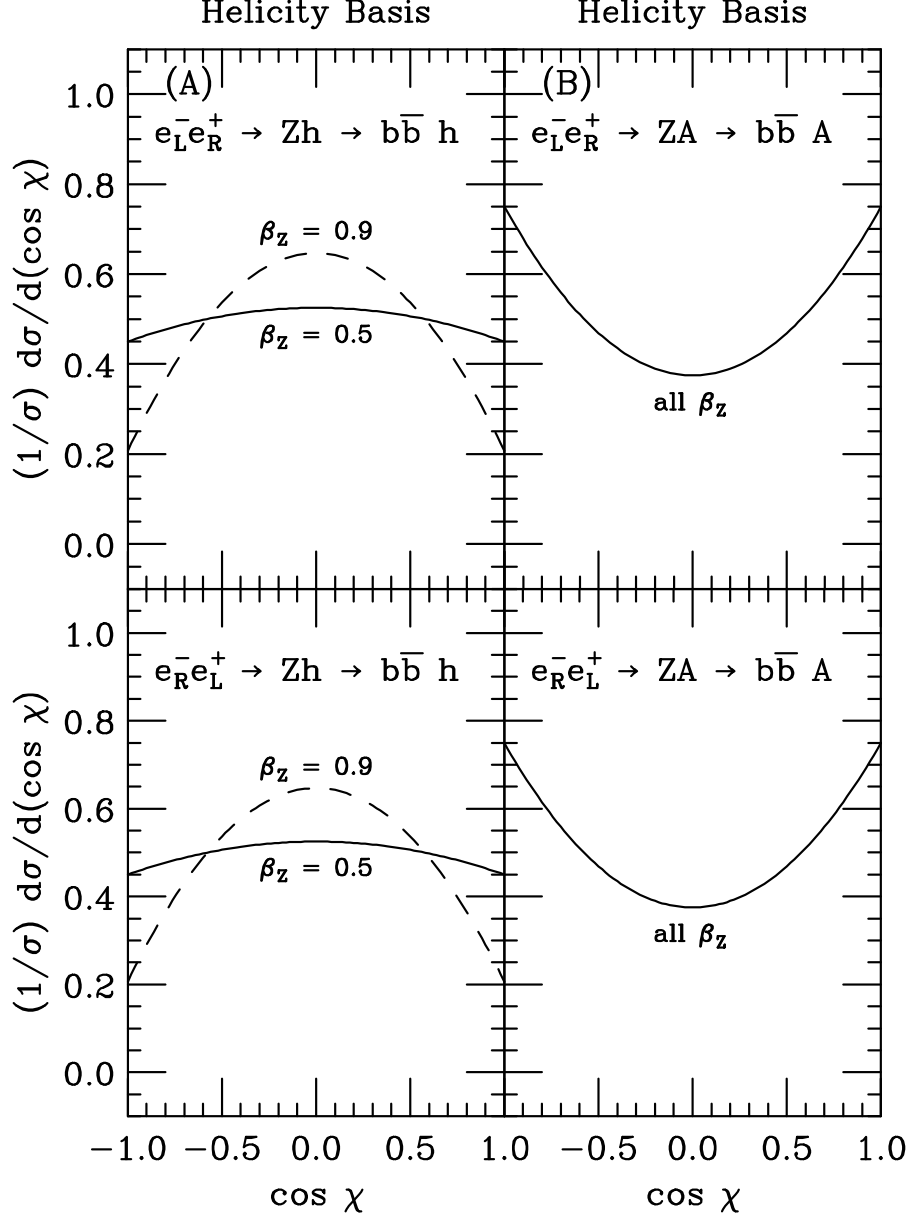


FIG. 11:  $Z$  decay angular distributions in the ZMF helicity basis for **(A)**  $e^+e^- \rightarrow Zh \rightarrow b\bar{b}h$  and **(B)**  $e^+e^- \rightarrow ZA \rightarrow b\bar{b}A$ . The decay angle  $\chi$  is defined as the angle in the  $Z$  rest frame between the spin axis direction and the direction of motion of the negatively-charged lepton.

### B. $Zh$ in the $Zh$ -transverse basis

We now turn to the  $Zh$ -transverse basis, Eq. (12), which was engineered to eliminate the longitudinal  $Z$  bosons from the mix. Consequently, we obtain a decay angular distribution

of the form

$$\frac{1}{\sigma_L} \frac{d\sigma_L}{d(\cos \chi)} \Big|_{\text{trans}} = \frac{3}{8}(\cos^2 \chi + 1) + \frac{9}{8} \frac{q_{fL}^2 - q_{fR}^2}{q_{fL}^2 + q_{fR}^2} \frac{\cos \chi}{3 - 2\beta_z^2} \left(1 - \beta_z^2 + \frac{\arcsin \beta_z}{\gamma_z \beta_z}\right). \quad (55)$$

A plot of this distribution appears in the panels on the left side of Fig. 12. Eq. (55) simplifies near threshold ( $\beta_z \rightarrow 0$ ) and in the ultra-relativistic limit ( $\beta_z \rightarrow 1$ ) as follows:

$$\begin{aligned} \frac{1}{\sigma_L} \frac{d\sigma_L}{d(\cos \chi)} \Big|_{\text{trans}} &\longrightarrow \frac{3}{8}(\cos^2 \chi + 1) + \frac{3}{4} \frac{q_{fL}^2 - q_{fR}^2}{q_{fL}^2 + q_{fR}^2} \cos \chi [1 + \mathcal{O}(\beta_z^4)] & (\beta_z \rightarrow 0) \\ &\longrightarrow \frac{3}{8}(\cos^2 \chi + 1) & (\beta_z \rightarrow 1). \end{aligned} \quad (56)$$

Notice that in contrast to the result in the helicity basis, even near threshold this distribution displays non-trivial correlations. The shape of this distribution is a rather weak function of the machine energy.

### C. $ZA$ in the helicity basis

Repeating the calculation with the pseudoscalar spin functions instead, we obtain the result for  $ZA$  production and decay in the helicity basis:

$$\frac{1}{\sigma_L} \frac{d\sigma_L}{d(\cos \chi)} \Big|_{\text{helicity}} = \frac{3}{8}(1 + \cos^2 \chi). \quad (57)$$

This angular distribution is plotted in the panels on the right-hand side of Fig. 11. There is no forward-backward asymmetry in Eq. (57) due to the equal mix of ( $\uparrow$ ) and ( $\downarrow$ ) spin states in this basis. Furthermore, since we have used a fixed value of  $\xi$  and the spin functions contain no  $\beta_z$  dependence themselves, the result in Eq. (57) holds for all machine energies and all boson masses (provided, of course, that the  $ZA$  final state is kinematically allowed).

### D. $ZA$ in the $Zh$ -transverse basis

Since we won't know *a priori* what sort of Higgs we are dealing with, we also present the  $ZA$  decay angular distribution in the (“wrong”)  $Zh$ -transverse basis:

$$\begin{aligned} \frac{1}{\sigma_L} \frac{d\sigma_L}{d(\cos \chi)} \Big|_{\text{trans}} &= (1 + \cos^2 \chi) \left[ \frac{3}{32} - \frac{9}{64} \frac{1 - \beta_z^2}{\beta_z^2} \left( \frac{1}{\beta_z} \ln \frac{1 - \beta_z}{1 + \beta_z} + 2 \right) \right] \\ &\quad + \frac{9}{32} \sin^2 \chi \left[ \frac{2}{\beta_z^2} + \frac{1 - \beta_z^2}{\beta_z^3} \ln \frac{1 - \beta_z}{1 + \beta_z} \right] \end{aligned}$$

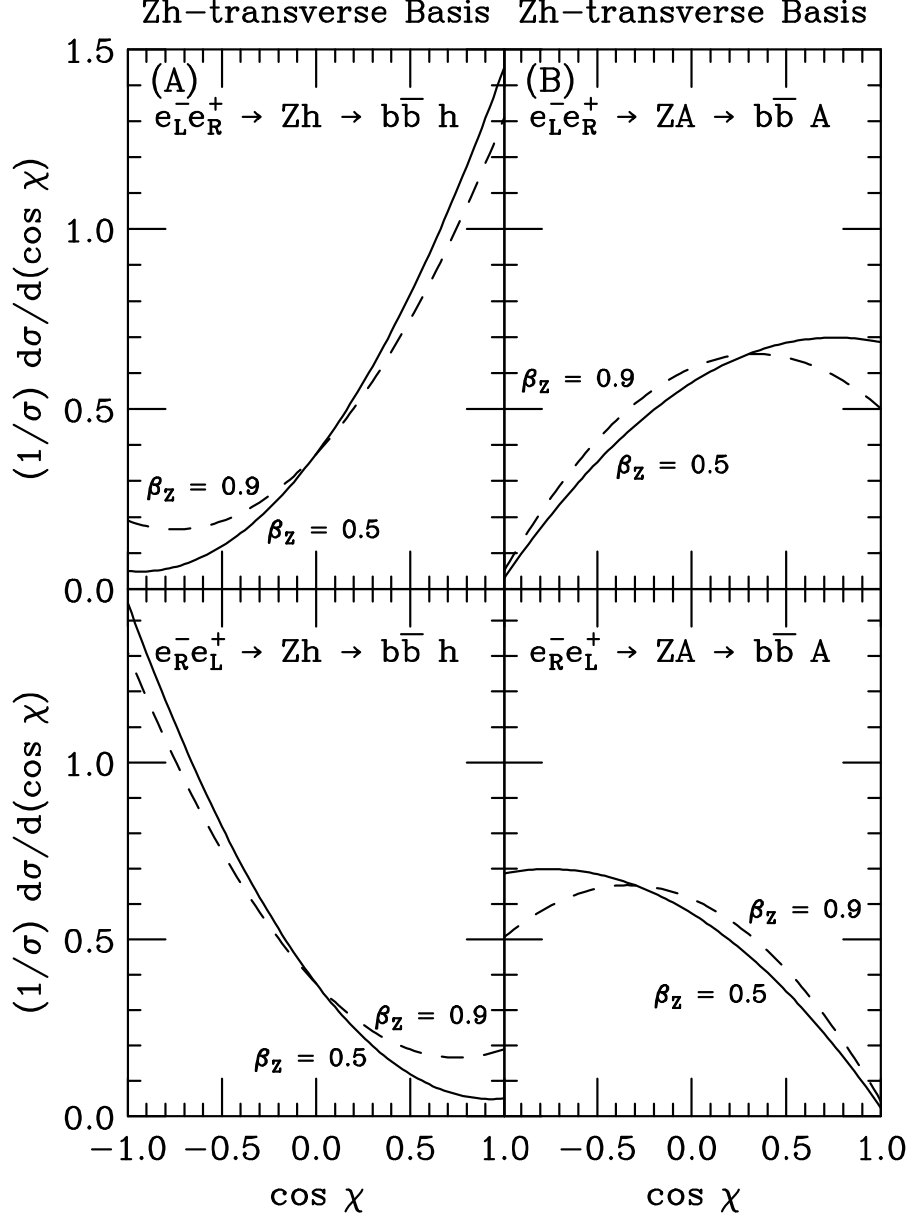


FIG. 12:  $Z$  decay angular distributions in the  $Zh$ -transverse basis for **(A)**  $e^+e^- \rightarrow Zh \rightarrow b\bar{b}h$  and **(B)**  $e^+e^- \rightarrow ZA \rightarrow b\bar{b}A$ . The decay angle  $\chi$  is defined as the angle in the  $Z$  rest frame between the spin axis direction and the direction of motion of the negatively-charged lepton.

$$-\frac{9}{16} \frac{q_{fL}^2 - q_{fR}^2}{q_{fL}^2 + q_{fR}^2} \cos \chi \sqrt{1 - \beta_z^2} \frac{1}{\beta_z^2} \left[ 1 - \beta_z^2 - \frac{\arcsin \beta_z}{\beta_z \gamma_z} \right]. \quad (58)$$

A plot of this angular distribution appears in Fig. 12B. Eq. (58) looks somewhat complicated because it employs a spin basis designed to simplify the  $Zh$  amplitude, not the  $ZA$  amplitude.

All of the  $\beta_Z$ -dependence contained in Eq. (58) is a consequence of choosing  $\xi$  to be an explicit function of  $\beta_Z$  [*cf.* Eq. (12)].

### E. Comparison of $Zh$ and $ZA$

We now turn to a direct comparison between the decay angular distributions for  $Zh$  and  $ZA$  in both the helicity and  $Zh$ -transverse bases. From Fig. 13 we see that, when the  $Zh$ -transverse basis is used, there are regions of the  $\cos \chi$  distribution where the expected number of events differs by as much as a factor of 2. In contrast, when the helicity basis is used, the maximum difference in expected number of events is never that large.

A second feature of this plot which has the potential to be used in distinguishing  $Zh$  from  $ZA$  is a number we will call the “ $\cos \chi$  forward-backward asymmetry ratio”,  $\mathcal{Z}$ :

$$\mathcal{Z} \equiv \frac{\int_0^1 d(\cos \chi) \frac{1}{\sigma_L} \frac{d\sigma_L}{d(\cos \chi)}}{\int_{-1}^0 d(\cos \chi) \frac{1}{\sigma_L} \frac{d\sigma_L}{d(\cos \chi)}}. \quad (59)$$

In plain English,  $\mathcal{Z}$  is the ratio of the number of events with  $\cos \chi > 0$  to the number of events with  $\cos \chi < 0$ . We may use the expressions contained in Eqs. (34), (35), and (52) to rewrite this in terms of the coupling constants for the chosen  $Z$  decay mode and the fractions of spin-( $\uparrow$ ) and spin-( $\downarrow$ )  $Z$  bosons:

$$\mathcal{Z} = \frac{4 + 3 \frac{q_{fL}^2 - q_{fR}^2}{q_{fL}^2 + q_{fR}^2} (f^+ - f^-)}{4 - 3 \frac{q_{fL}^2 - q_{fR}^2}{q_{fL}^2 + q_{fR}^2} (f^+ - f^-)}. \quad (60)$$

We see from Eq. (60) that two ingredients are necessary to have  $\mathcal{Z} \neq 1$ : first, we need charge/flavor identification in the final state of the  $Z$ 's (see the last line of Table IV). Second, we need the fraction of spin-( $\uparrow$ )  $Z$  bosons ( $f^+$ ) to differ from the fraction of spin-( $\downarrow$ )  $Z$  bosons ( $f^-$ ). We point this out because in the helicity basis, both  $Zh$  and  $ZA$  production have equal numbers of spin-( $\uparrow$ ) and spin-( $\downarrow$ )  $Z$  bosons. Hence

$$\mathcal{Z}_{\text{helicity}}^{Zh} = 1; \quad \mathcal{Z}_{\text{helicity}}^{ZA} = 1, \quad (61)$$

*i.e.* in the helicity basis, measuring the value of  $\mathcal{Z}$  does not distinguish between  $Zh$  and  $ZA$ . On the other hand, in the  $Zh$ -transverse basis, the values in Tables II and III tell us that

$$\mathcal{Z}_{\text{trans}}^{Zh} = 5.54; \quad \mathcal{Z}_{\text{trans}}^{ZA} = 1.95, \quad (62)$$

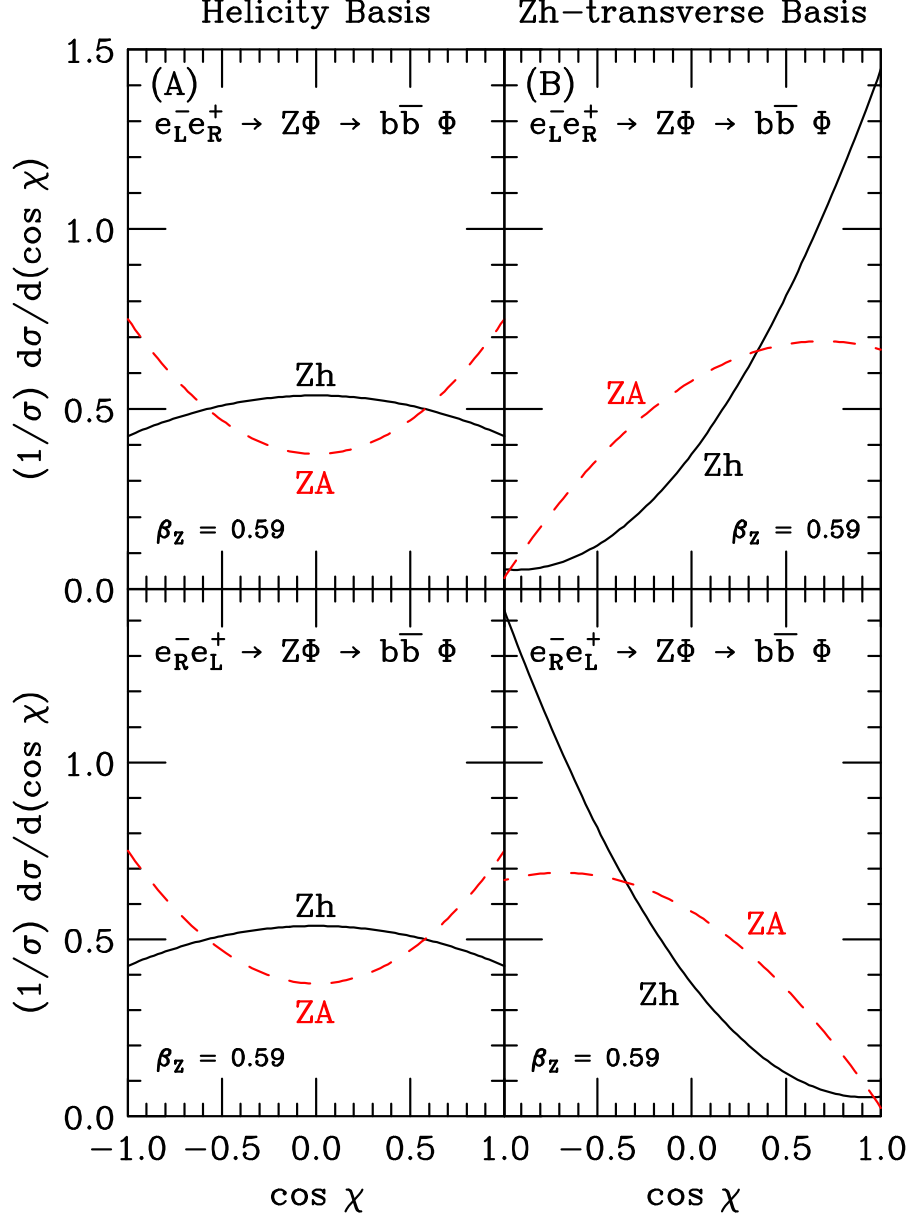


FIG. 13: Comparison of  $Z$  decay angular distributions for **(A)**  $e^+e^- \rightarrow Zh \rightarrow b\bar{b}h$  and **(B)**  $e^+e^- \rightarrow ZA \rightarrow b\bar{b}A$  for  $\beta_z = 0.59$  ( $M_h = 120$  GeV,  $\sqrt{s} = 250$  GeV) in the helicity and  $Zh$ -transverse bases. The decay angle  $\chi$  is defined as the angle in the  $Z$  rest frame between the spin axis direction and the direction of motion of the negatively-charged lepton.



*i.e.* in the  $Zh$ -transverse basis,  $\mathcal{Z}$  is a potentially very useful measure that can distinguish  $Zh$  from  $ZA$ .

Because the optimal spin basis for studying  $Zh$  production and decay is not the same as the optimal basis for studying  $ZA$  production and decay, it is not clear at this stage exactly which route is the best one to pursue. (See Appendix C for a discussion of the beamline basis. Depending on the machine energy, the beamline basis provides a competitive alternative to the  $Zh$ -transverse basis and may possess smaller systematic uncertainties.) Optimization of the method requires a detailed detector simulation. Nevertheless, it is clear that a sound strategy would involve utilizing all possible sources of information about distributions that differ between the two processes. For example, the turn-on of the cross section as the machine energy is raised above threshold is different for  $Zh$  and  $ZA$  production (Eq. (17) versus Eq. (28); also Ref. [1]).

A second distinguishing characteristic of the two processes is the radically different  $\xi$ -dependence of the  $Zh$  and  $ZA$  amplitudes. A measurement of the  $Z$  spin composition of a Higgs signal for different choices of  $\xi$  could be used to provide one piece of evidence relating to the correct assignment of  $\mathcal{J}^{PC}$  quantum numbers to the state. In particular, it would be useful to measure the fraction of longitudinally polarized  $Z$ 's in a sample of  $Z$ -Higgs candidates in using both the helicity and  $Zh$ -transverse bases. For the signal events, a scalar Higgs should show no longitudinal  $Z$ 's in the  $Zh$ -transverse basis, while for a pseudoscalar Higgs the longitudinal  $Z$  fraction would be in the 50%–75% range, depending on the machine energy. Although one should really do a full detector simulation to be sure (the systematics associated with each basis will be different), we believe that the difference between 50% and 0 should be large enough to be observable with only modest detector sensitivity.

## F. $CP$ -Violating Higgs Bosons

Once the additional structure necessary to generate a  $CP$ -odd Higgs boson has been introduced into the Lagrangian, it is a small step to incorporate some level of  $CP$ -violation in the scalar sector [16]. Rather than attempt an exhaustive survey of all of the possible mechanisms and models, we will briefly consider possibility that the Higgs mass eigenstate is not a  $CP$ -eigenstate, and describe how this would affect the angular distributions we have been discussing in this paper.

In particular, we imagine that the physical Higgs mass eigenstates are a linear combination of the  $CP$ -even and  $CP$ -odd states:

$$\begin{aligned}\phi_1 &\equiv h \cos \psi + A \sin \psi \\ \phi_2 &\equiv -h \sin \psi + A \cos \psi,\end{aligned}\tag{63}$$

where  $\psi$  is an effective mixing angle, defined such that when  $\psi = 0$ , the state  $\phi_1$  is purely  $CP$ -even and  $\phi_2$  purely  $CP$ -odd.

If the only source of  $CP$ -violation in the Higgs sector is through the mixing in Eq. (63), then it is straightforward to see how the effects will turn up in the  $\cos \chi$  (or other) distribution. That is, the result will be a linear combination of the  $Zh$  and  $ZA$  distributions weighted by coefficients that are sensitive to the mixing angle  $\psi$ . Thus, if we look at a distribution (such as  $d\sigma/d(\cos \chi)$  using the  $Zh$ -transverse basis) for which the pure  $Zh$  and  $ZA$  predictions differ significantly, information on the value of  $\psi$  can be extracted by a fit to this distribution. The advantage of this method is that this measurement can be performed without even looking at how the Higgs decays. Since  $Z$  decays are well-understood, any deviations from the  $CP$ -conserving predictions contained in Eqs. (55), (58), and (62) can be unambiguously attributed to the  $CP$ -quantum numbers (or lack thereof) of the ‘‘Higgs’’.

## VII. CONCLUSIONS

Once the Higgs boson is discovered, it will be important to check its properties to see if its spin-parity-charge-conjugation quantum numbers are indeed  $\mathcal{J}^{PC} = 0^{++}$  as predicted by the Standard Model, or if some other set of values (for example,  $\mathcal{J}^{PC} = 0^{+-}$ ) applies. As with any physics measurement, it is best to have multiple approaches so that consistency checks may be performed.

In this paper we have discussed distinguishing between the associated production of a scalar ( $0^{++}$ ) Higgs boson with a  $Z$  boson and the associated production of a (so-called) pseudoscalar ( $0^{+-}$ ) Higgs boson with a  $Z$  boson. As noted in Ref. [1], the total cross sections for the two processes have different energy dependences near threshold: see Eqs. (18) and (29). Furthermore, the production-angle distribution for the  $Zh$  process is proportional to  $1 - \frac{1}{2}\beta_Z^2(1 + \cos^2 \theta^*)$  [2]: that is, it is flat near threshold ( $\beta_Z \rightarrow 0$ ), and develops a  $1 - \cos^2 \theta^*$  shape at high energies ( $\beta_Z \rightarrow 1$ ). On the other hand, in the  $ZA$  case the shape

of this distribution is  $1 + \cos^2 \theta^*$ , irrespective of energy.

The primary focus of this paper and an additional means of distinguishing  $Zh$  production from  $ZA$  production is provided by the decay-angular distributions of the  $Z$  boson illustrated in Fig. 13. This approach has two distinct advantages: both of which stem from looking at the  $Z$  rather than the Higgs. First, it provides a method that does not depend on the existence of a particular Higgs decay mode with a sufficiently large branching ratio. In fact, this method does not require observation of the Higgs decay products at all! The second main advantage is that  $Z$  decays are well-understood. Thus, examining the spin state of the  $Z$  can provide unambiguous information about the type of Higgs boson it was produced with. In this connection, unless the collider center-of-mass energy is large enough so that the  $Z$ 's are ultra-relativistic, it is fruitful to investigate other choices for the  $Z$ -boson spin basis besides the traditional helicity basis. In particular, the  $Zh$ -transverse basis, defined in Eq. (12), is potentially useful since  $Zh$  events should contain **no** longitudinal  $Z$ 's whereas the fraction of longitudinal  $Z$ 's in  $ZA$  events is over 50% (see Tables II and III). This measurement benefits from having polarized beams. In particular, for the combination of Higgs mass ( $M_h=120$  GeV) and machine energy ( $\sqrt{s} = 250$  GeV) highlighted in this paper, more than 99% of the  $Z$  bosons in the  $e_L^- e_R^+ \rightarrow Zh$  process are in the  $(\uparrow)$  spin state when the  $Zh$ -transverse spin basis is used. This is very close to the “ideal” situation where all of the  $Z$ 's are produced with the same spin projection and leads to angular correlations which are very nearly as large as theoretically possible. Large angular correlations are well-suited to defining quantities like the  $\cos \chi$  forward-backward asymmetry ratio, Eq. (59), that are sensitive to the  $CP$ -eigenvalue of the Higgs boson. In the helicity basis, this ratio is predicted to be unity for both  $Zh$  and  $ZA$  production whereas in the  $Zh$  transverse basis we predict a significant difference in this ratio between  $Zh$  and  $ZA$  production.

## Acknowledgments

The Fermi National Accelerator Laboratory is operated by Universities Research Association, Inc., under contract DE-AC02-76CHO3000 with the U.S. Department of Energy. We would like to thank Peter Fisher and Philip Bambade for illuminating discussions. GM would like to thank Mike Doncheski for helpful discussions, and the FNAL theory group for their kind hospitality during visits to concentrate on this work. Additional support for GM

for this work was provided through a Research Development Grant from the Commonwealth College of the Pennsylvania State University.

## APPENDIX A: ROLE OF INTERFERENCE TERMS

Suppose that one could find a spin basis where the  $Z$ 's are produced in a single spin state  $\lambda_0$ . Then, the full production and decay distribution could be computed from

$$d\sigma \sim |\mathcal{M}_{\lambda_0} \mathcal{D}_{\lambda_0}|^2. \quad (\text{A1})$$

The interpretations of the pieces of Eq. (A1) are obvious:  $\mathcal{M}_{\lambda_0}$  is the amplitude for producing the  $Z$  with spin  $\lambda_0$  in association with the Higgs;  $\mathcal{D}_{\lambda_0}$  is the amplitude describing the decay of the  $Z$  with spin  $\lambda_0$ .

Of course, no such basis exists (although, as pointed out above, the  $Zh$ -transverse basis comes very close). So, what we really have is of the form

$$d\sigma \sim \left| \sum_{\lambda} \mathcal{M}_{\lambda} \mathcal{D}_{\lambda} \right|^2. \quad (\text{A2})$$

Our (semi-classical) intuition would like us to interpret this result as the sum over all possible spin states of the probability to produce the given spin state multiplied by its decay probability. The difference between Eq. (A2) and the expression representing our intuition is

$$\mathcal{I} \equiv \left| \sum_{\lambda} \mathcal{M}_{\lambda} \mathcal{D}_{\lambda} \right|^2 - \sum_{\lambda} \left| \mathcal{M}_{\lambda} \mathcal{D}_{\lambda} \right|^2. \quad (\text{A3})$$

The contributions on the right hand side of Eq. (A3) are precisely the quantum interference terms present in the coherent sum (A2). When these interference terms are small, the contribution to the full production and decay distribution fits our semi-classical intuition. On the other hand, when Eq. (A3) is large, quantum interference effects become important, and our semi-classical intuition falls short.

Thus, one way to judge the quality of a particular spin basis is to examine the relative importance of the interference terms in the production and decay distribution. We normalize the interference sum to the total matrix element on a point-by-point basis,

$$\hat{\mathcal{I}} \equiv \frac{\left| \sum_{\lambda} \mathcal{M}_{\lambda} \mathcal{D}_{\lambda} \right|^2 - \sum_{\lambda} \left| \mathcal{M}_{\lambda} \mathcal{D}_{\lambda} \right|^2}{\left| \sum_{\lambda} \mathcal{M}_{\lambda} \mathcal{D}_{\lambda} \right|^2} \quad (\text{A4})$$

and then determine the distribution in  $\hat{\mathcal{I}}$ . For a process containing  $N$  independent intermediate spin configurations,  $\hat{\mathcal{I}}$  can range from  $-\infty$  (total destructive interference) to  $(N-1)/N$

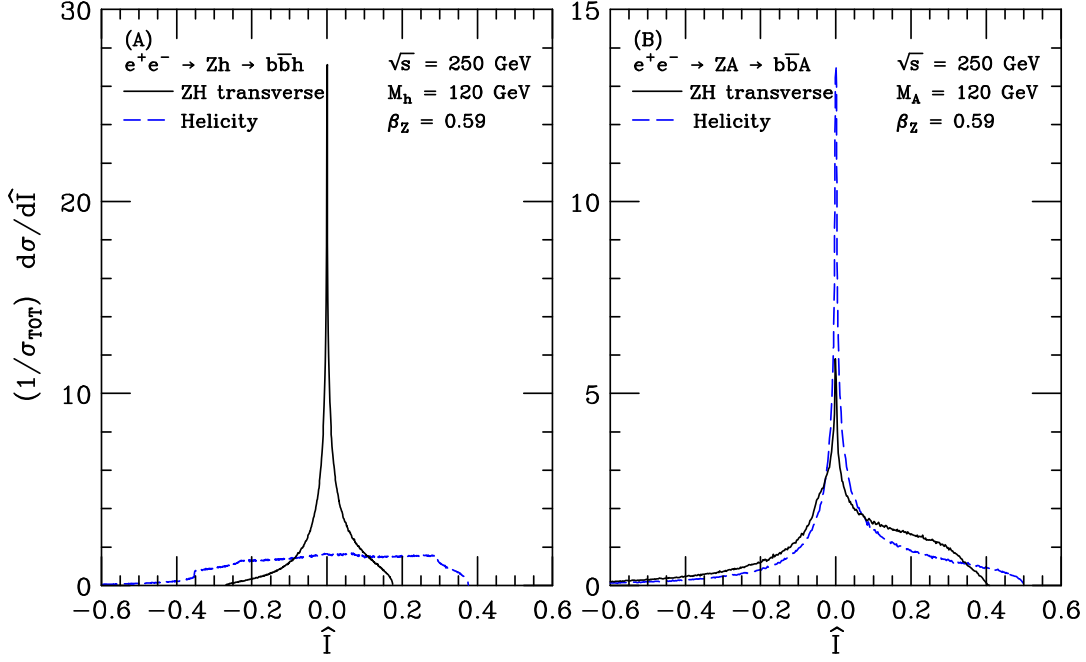


FIG. 14: The relative importance of the interference terms in the  $Zh$ -transverse and helicity bases at  $\sqrt{s} = 250$  GeV and  $m_h = 120$  GeV ( $\beta_z = 0.59$ ) for (A)  $e^+e^- \rightarrow Zh \rightarrow b\bar{b}h$  and (B)  $e^+e^- \rightarrow ZA \rightarrow b\bar{b}A$ . Plotted is the differential distribution in  $\hat{\mathcal{I}}$ , the value of the interference term normalized to the square of the total matrix element.

(total constructive interference). Clearly, in the simple case represented by Eq. (A1) where there is no interference, this distribution will be a delta function centered at  $\hat{\mathcal{I}} = 0$ . In the more general situation represented by Eq. (A2), a plot of  $d\sigma/d\hat{\mathcal{I}}$  displays the relative importance of the various values of  $\hat{\mathcal{I}}$ .

With these considerations in mind, we present Fig. 14, comparing the distribution in  $\hat{\mathcal{I}}$  for the unpolarized processes  $e^+e^- \rightarrow Zh \rightarrow b\bar{b}h$  and  $e^+e^- \rightarrow ZA \rightarrow b\bar{b}A$  using the  $Zh$ -transverse and helicity bases, and assuming that  $M_h = 120$  GeV and  $\sqrt{s} = 250$  GeV ( $\beta_z = 0.59$ ). Fig. 14A shows that the removal from  $Zh$  production of the longitudinal  $Z$ 's with their relatively wide distribution in  $\cos\chi$  leads to a greatly reduced role for the interference terms in the  $Zh$ -transverse basis as compared to the helicity basis. In fact, nearly 85% of the total cross section is accounted for by the  $|\hat{\mathcal{I}}| < 0.10$  region when using the  $Zh$ -transverse basis: this is a reasonably narrow distribution. On the other hand, since

TABLE V: Fraction of the  $e^+e^- \rightarrow Zh \rightarrow b\bar{b}h$  cross section coming from phase space points where the interference term is less than or equal to some cutoff assuming a Higgs mass of 120 GeV and a machine center-of-mass energy of 250 GeV ( $\beta_z = 0.59$ ).

Integration region	Helicity basis	$Zh$ -transverse basis
$ \hat{\mathcal{I}}  < 0.05$	0.159	0.640
$ \hat{\mathcal{I}}  < 0.10$	0.311	0.844
$ \hat{\mathcal{I}}  < 0.15$	0.454	0.950
$ \hat{\mathcal{I}}  < 0.20$	0.595	0.987
$ \hat{\mathcal{I}}  < 0.25$	0.734	0.998

TABLE VI: Fraction of the  $e^+e^- \rightarrow ZA \rightarrow b\bar{b}A$  cross section coming from phase space points where the interference term is less than or equal to some cutoff assuming a Higgs mass of 120 GeV and a machine center-of-mass energy of 250 GeV ( $\beta_z = 0.59$ ).

Integration region	Helicity basis	$Zh$ -transverse basis
$ \hat{\mathcal{I}}  < 0.05$	0.406	0.291
$ \hat{\mathcal{I}}  < 0.10$	0.561	0.461
$ \hat{\mathcal{I}}  < 0.15$	0.662	0.589
$ \hat{\mathcal{I}}  < 0.20$	0.737	0.695
$ \hat{\mathcal{I}}  < 0.25$	0.797	0.785

all three spin states contain significant populations in the helicity basis, the interference terms tend to be large a significant fraction of the time; in fact, only 31% of the cross section comes from configurations where  $|\hat{\mathcal{I}}| < 0.10$ . In Table V we have tabulated the fraction of the total cross section contributed by regions where  $|\hat{\mathcal{I}}| < 0.05, 0.10, 0.15, 0.20$ , and 0.25 in these two bases.

Fig. 14B displays the same information for the  $e^+e^- \rightarrow ZA \rightarrow b\bar{b}A$  case. In this situation, the contrast between the “right” (helicity) and “wrong” ( $Zh$ -transverse) bases is less dramatic: both choices of spin basis contain significant contributions from regions

where the interference terms are large: in particular, both distributions exhibit long tails in the  $\widehat{\mathcal{I}} < 0$  (destructive interference) region. From Table VI we learn that the range  $|\widehat{\mathcal{I}}| < 0.10$  contributes 56% of the total cross section in the helicity basis but only 46% in the  $Zh$ -transverse basis.



## APPENDIX B: LORENTZ-COVARIANT FORM

Even when we include the decay of the  $Z$  boson, the Lorentz-invariant result for the square of the matrix element for associated Higgs production is surprisingly simple. If we let each particle's 4-momentum be represented by its symbol ( $e \equiv e^-$  and  $\bar{e} \equiv e^+$ ), then we obtain

$$\left| \mathcal{M}(e_L^- e_R^+ \rightarrow Zh \rightarrow f \bar{f} h) \right|^2 \sim 4q_{eL}^2 \left[ q_{fL}^2 (2\bar{e} \cdot f)(2e \cdot \bar{f}) + q_{fR}^2 (2e \cdot f)(2\bar{e} \cdot \bar{f}) \right] \quad (\text{B1})$$

and

$$\left| \mathcal{M}(e_R^- e_L^+ \rightarrow Zh \rightarrow f \bar{f} h) \right|^2 \sim 4q_{eR}^2 \left[ q_{fL}^2 (2e \cdot f)(2\bar{e} \cdot \bar{f}) + q_{fR}^2 (2\bar{e} \cdot f)(2e \cdot \bar{f}) \right]. \quad (\text{B2})$$

for a  $CP$ -even Higgs. The results for a  $CP$ -odd Higgs are not quite as compact as Eqs. (B1) and (B2), primarily because of the momentum-dependent Levi-Cevita-tensor vertex:

$$\begin{aligned} \left| \mathcal{M}(e_L^- e_R^+ \rightarrow ZA \rightarrow f \bar{f} A) \right|^2 \sim & q_{eL}^2 q_{fL}^2 \left\{ (2e \cdot \bar{e})(2f \cdot \bar{f}) \left[ (2f \cdot \bar{e})^2 + (2e \cdot \bar{f})^2 \right. \right. \\ & \left. \left. + 2(2e \cdot f)(2\bar{e} \cdot \bar{f}) - (2e \cdot \bar{e})(2f \cdot \bar{f}) \right] \right. \\ & \left. - \left[ (2e \cdot \bar{f})(2f \cdot \bar{e}) - (2e \cdot f)(2\bar{e} \cdot \bar{f}) \right]^2 \right\} \\ & + q_{eL}^2 q_{fR}^2 \left\{ (2e \cdot \bar{e})(2f \cdot \bar{f}) \left[ (2e \cdot f)^2 + (2\bar{e} \cdot \bar{f})^2 \right. \right. \\ & \left. \left. + 2(2\bar{e} \cdot f)(2e \cdot \bar{f}) - (2e \cdot \bar{e})(2f \cdot \bar{f}) \right] \right. \\ & \left. - \left[ (2e \cdot f)(2\bar{e} \cdot \bar{f}) - (2e \cdot \bar{f})(2\bar{e} \cdot f) \right]^2 \right\} \end{aligned} \quad (\text{B3})$$

$$\begin{aligned} \left| \mathcal{M}(e_R^- e_L^+ \rightarrow ZA \rightarrow f \bar{f} A) \right|^2 \sim & q_{eR}^2 q_{fL}^2 \left\{ (2e \cdot \bar{e})(2f \cdot \bar{f}) \left[ (2e \cdot f)^2 + (2\bar{e} \cdot \bar{f})^2 \right. \right. \\ & \left. \left. + 2(2\bar{e} \cdot f)(2e \cdot \bar{f}) - (2e \cdot \bar{e})(2f \cdot \bar{f}) \right] \right. \\ & \left. - \left[ (2e \cdot f)(2\bar{e} \cdot \bar{f}) - (2e \cdot \bar{f})(2\bar{e} \cdot f) \right]^2 \right\} \\ & + q_{eR}^2 q_{fR}^2 \left\{ (2e \cdot \bar{e})(2f \cdot \bar{f}) \left[ (2f \cdot \bar{e})^2 + (2e \cdot \bar{f})^2 \right. \right. \\ & \left. \left. + 2(2e \cdot f)(2\bar{e} \cdot \bar{f}) - (2e \cdot \bar{e})(2f \cdot \bar{f}) \right] \right. \\ & \left. - \left[ (2e \cdot \bar{f})(2f \cdot \bar{e}) - (2e \cdot f)(2\bar{e} \cdot \bar{f}) \right]^2 \right\}. \end{aligned} \quad (\text{B4})$$

## APPENDIX C: THE BEAMLINE BASIS

Another potentially interesting basis is the beamline basis [9], which is defined by

$$\sin \xi = \frac{\gamma_z^{-1} \sin \theta^*}{1 - \beta_z \cos \theta^*}; \quad \cos \xi = \frac{\cos \theta^* - \beta_z}{1 - \beta_z \cos \theta^*}. \quad (\text{C1})$$

Here  $\beta_z$  is the ZMF speed of the  $Z$  boson. In this basis, the spin axis for the  $Z$  is the electron direction. Because the beam directions are experimentally well-determined, any angular measurement uncertainty issues in this basis should be very different than those in the helicity or  $Zh$ -transverse bases.

Figure 15 displays the relationship between  $\cos \xi$  and  $\cos \theta^*$  in the beamline,  $Zh$ -transverse and helicity bases for low ( $\beta_z = 0.11$ ), medium ( $\beta_z = 0.59$ ) and high ( $\beta_z = 0.92$ ) values of the ZMF speed of the  $Z$  boson. Near threshold ( $\beta_z \rightarrow 0$ ), the beamline basis is nearly coincident with the  $Zh$ -transverse basis. In the other extreme ( $\beta_z \rightarrow 1$ ), the beamline basis becomes coincident with the helicity basis. Between these two extremes, the beamline basis interpolates between these two bases.

Figure 16 illustrates the breakdown of the  $Zh$  and  $ZA$  production cross sections at  $\beta_z = 0.59$  into the various  $Z$  spin states as a function of the production angle in the ZMF for both possible polarizations of the colliding beams. Numerical values for these fractions for a Higgs mass of 120 GeV and a collider center-of-mass energy of 250 GeV  $\sqrt{s} = 250$  GeV are presented in Table VII. Recall that the helicity basis is optimal for pseudoscalar production and that, as shown on Fig. 15, the beamline basis is far from the helicity basis at this energy. Thus, it is not surprising to find significant contributions from all three spin states to the  $ZA$  cross section. On the other hand, for  $Zh$  production, the beamline basis does zero out one of the transverse spin states when polarized beams are used.

Fig. 17 illustrates the evolution of the spin fractions in the beamline basis as the machine energy is changed. Amusingly, one of the two transverse spin components is always equal to 50% in this basis for  $ZA$  production, with the remainder divided between the other transverse spin and the longitudinal component.

The explicit form of the spin functions in the beamline basis read

$$\begin{aligned} \mathcal{S}_L^+ &= \gamma_z^{-1} \sqrt{2} \\ \mathcal{S}_L^- &= 0 \\ \mathcal{S}_L^0 &= \beta_z s_\theta \end{aligned} \quad (\text{C2})$$

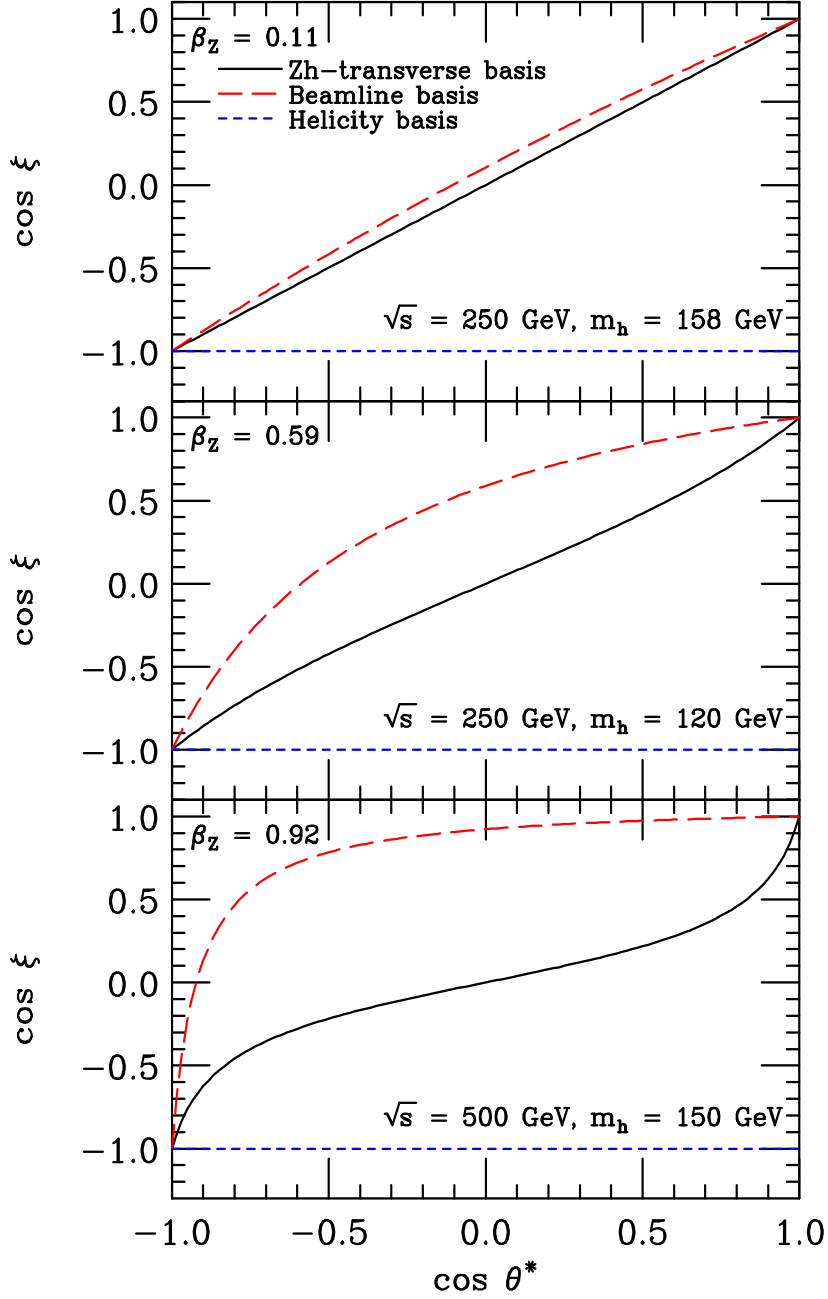


FIG. 15: The relationship between  $\cos \xi$  and  $\cos \theta^*$  in the  $Zh$ -transverse (solid), beamline (long dashes), and helicity (short dashes) bases at  $\beta_z = 0.11, 0.59$ , and  $0.92$ . At small  $\beta_z$ , the beamline and  $Zh$ -transverse bases are approximately the same. For  $\beta_z \rightarrow 1$ , the beamline basis becomes the  $c_\xi = 1$  variant of the helicity basis while the  $Zh$ -transverse approaches the basis with  $c_\xi \equiv 0$ .

TABLE VII: Spin decompositions in the beamline basis for  $e^+e^- \rightarrow Z\phi$  assuming  $m_\phi = 120$  GeV and  $\sqrt{s} = 250$  GeV ( $\beta_z = 0.59$ ).

	(+)	(-)	(0)
$Zh$			
$e_L^- e_R^+$	84.8%	0.0%	15.2%
$e_R^- e_L^+$	0.0%	84.8%	15.2%
$e^- e^+$ (unpolarized)	48.6%	36.2%	15.2%
$ZA$			
$e_L^- e_R^+$	50.0%	8.3%	41.7%
$e_R^- e_L^+$	8.3%	50.0%	41.7%
$e^- e^+$ (unpolarized)	32.2%	26.1%	41.7%

for  $Zh$  production, and

$$\begin{aligned}
\tilde{\mathcal{S}}_L^+ &= \frac{1}{\sqrt{2}} \frac{2c_\theta - \beta_z(1 + c_\theta^2)}{1 - \beta_z c_\theta} \\
\tilde{\mathcal{S}}_L^- &= \frac{1}{\sqrt{2}} \frac{\beta_z s_\theta^2}{1 - \beta_z c_\theta} \\
\tilde{\mathcal{S}}_L^0 &= \frac{\gamma_z^{-1} s_\theta}{1 - \beta_z c_\theta}
\end{aligned} \tag{C3}$$

for  $ZA$  production.

Turning to the  $Z$  decay angular distributions discussed in Sec. VI, we obtain the following expressions in the beamline basis: first, for  $e_L^- e_R^+ \rightarrow Zh$

$$\begin{aligned}
\frac{1}{\sigma_L} \frac{d\sigma_L}{d(\cos \chi)} \Big|_{\text{beamline}} &= \frac{9}{8} \frac{1 - \beta_z^2}{3 - 2\beta_z^2} (1 + \cos^2 \chi) + \frac{3}{4} \frac{\beta_z^2}{3 - 2\beta_z^2} \sin^2 \chi \\
&\quad + \frac{9}{4} \frac{1 - \beta_z^2}{3 - 2\beta_z^2} \frac{q_{fL}^2 - q_{fR}^2}{q_{fL}^2 + q_{fR}^2} \cos \chi,
\end{aligned} \tag{C4}$$

and for  $e_L^- e_R^+ \rightarrow ZA$ :

$$\begin{aligned}
\frac{1}{\sigma_L} \frac{d\sigma_L}{d(\cos \chi)} \Big|_{\text{beamline}} &= \left\{ \frac{3}{32} + \frac{9}{32} \frac{1}{\beta_z^2} \left[ 2 - \beta_z^2 + \frac{\gamma_z^{-2}}{\beta_z} \ln \left( \frac{1 - \beta_z}{1 + \beta_z} \right) \right] \right\} (1 + \cos^2 \chi) \\
&\quad - \frac{9}{16} \frac{\gamma_z^{-2}}{\beta_z^2} \left[ 2 + \frac{1}{\beta_z} \ln \left( \frac{1 - \beta_z}{1 + \beta_z} \right) \right] \sin^2 \chi \\
&\quad - \frac{9}{16} \frac{q_{fL}^2 - q_{fR}^2}{q_{fL}^2 + q_{fR}^2} \frac{\gamma_z^{-2}}{\beta_z^2} \left[ 2 + \frac{1}{\beta_z} \ln \left( \frac{1 - \beta_z}{1 + \beta_z} \right) \right] \cos \chi,
\end{aligned} \tag{C5}$$

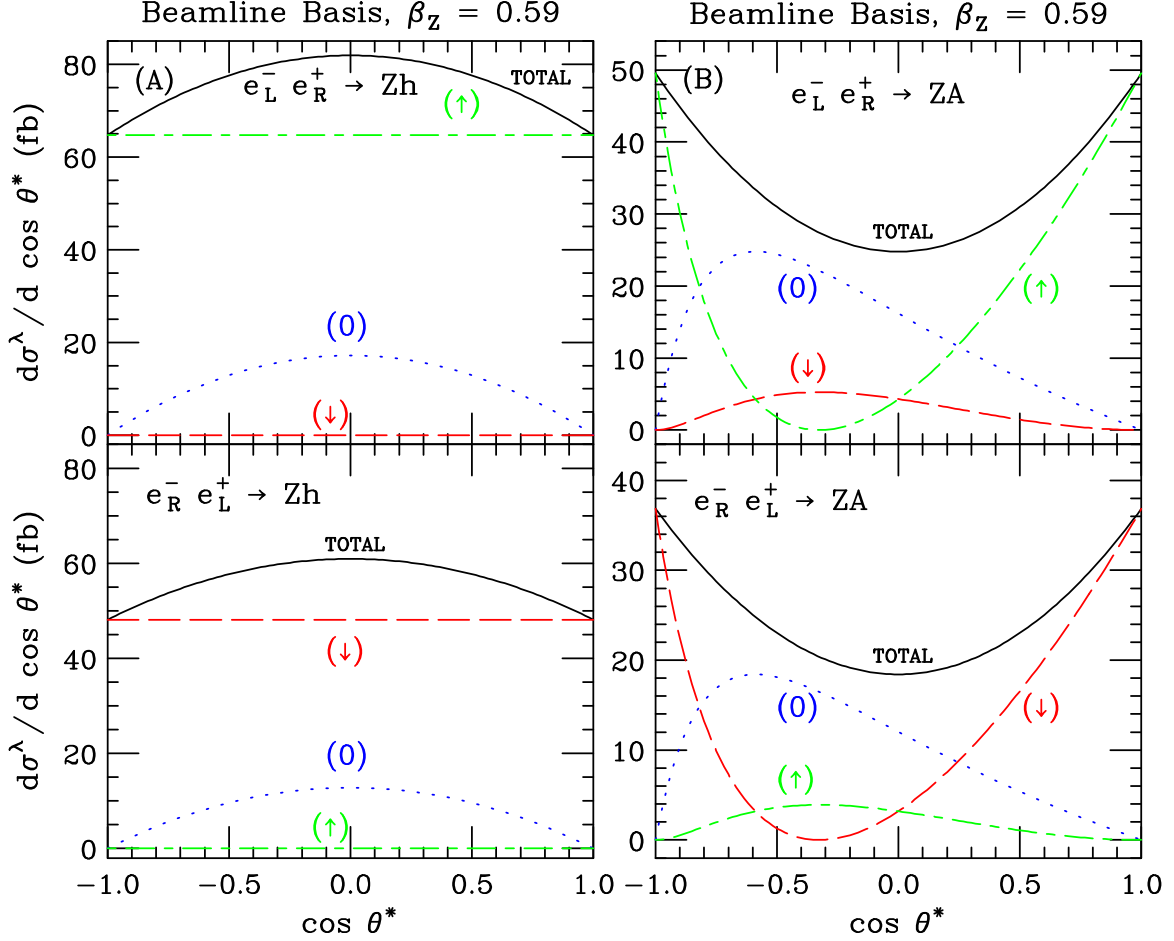


FIG. 16: Polarized production angle distributions for **(A)**  $e^+e^- \rightarrow Zh$  and **(B)**  $e^+e^- \rightarrow ZA$  assuming  $\sqrt{s} = 250$  GeV and  $M_h = 120$  GeV ( $\beta_z = 0.59$ ). Displayed are the contributions from the three possible  $Z$  spins in the beamline basis.

These distributions are displayed in Fig. 18 for both the scalar and pseudoscalar Higgs cases. For moderate  $\beta_z$ , the separation between  $Zh$  and  $ZA$  is nearly as good as in the  $Zh$ -transverse basis. The values of the  $\cos \chi$  forward-backward asymmetry ratio, Eq. (59), in the beamline basis are

$$\mathcal{Z}_{\text{beamline}}^{Zh} = 3.96; \quad \mathcal{Z}_{\text{beamline}}^{ZA} = 1.83. \quad (\text{C6})$$

Comparison to Eq. (62) reveals that in terms of this particular measure, the beamline basis performs nearly as well as the  $Zh$ -transverse basis.

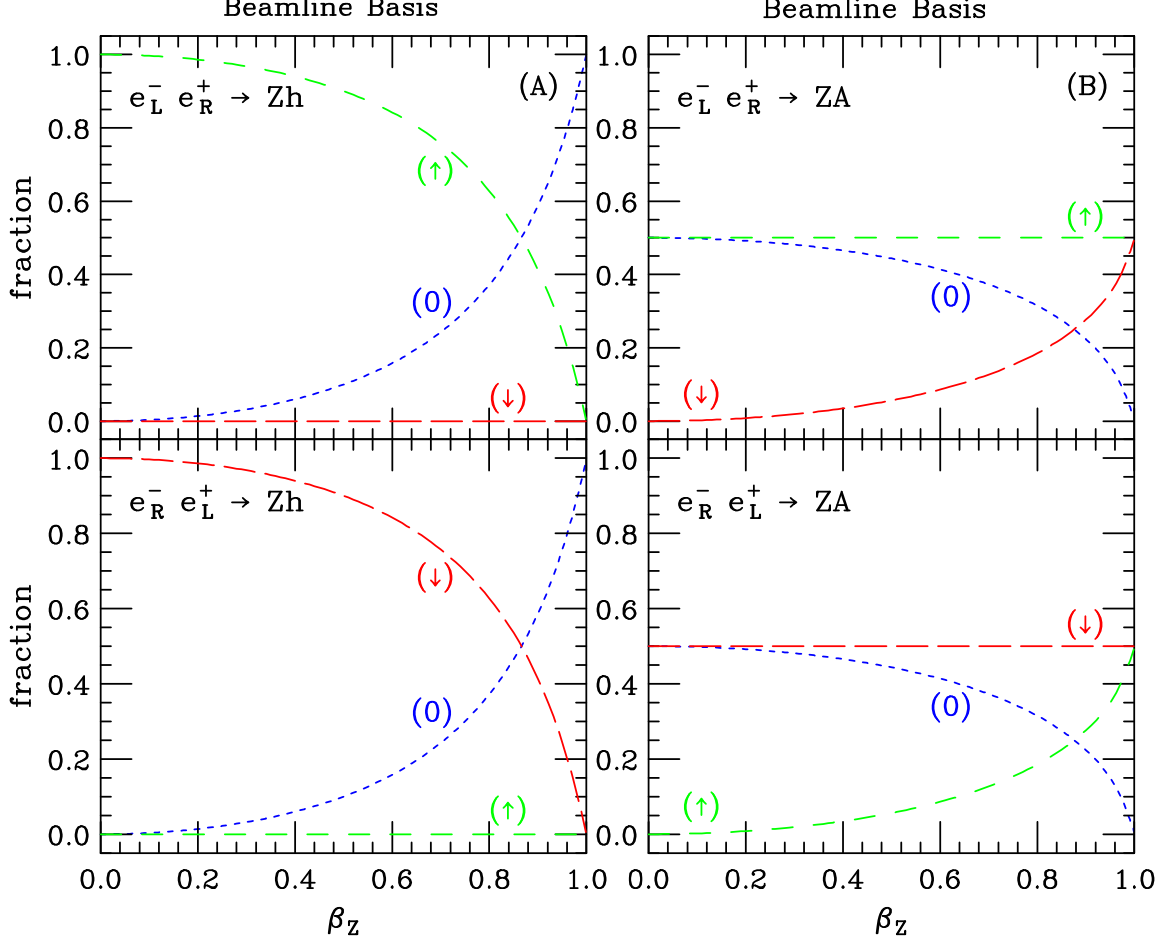


FIG. 17: Spin decomposition in the beamline basis of the polarized associated Higgs production cross sections as a function of the ZMF speed  $\beta_Z$  of the  $Z$  boson. Shown are the fractions of the total cross sections in the  $(\uparrow)$ ,  $(\downarrow)$ , and  $(0)$  spin states in **(A)**  $Zh$  and **(B)**  $ZA$  production. The beamline basis interpolates between the  $Zh$ -transverse basis at low  $\beta_Z$  and the helicity basis at high  $\beta_Z$  as can be seen by comparison with Figs. 5 and 7.

- 
- [1] D.J. Miller, S.Y. Choi, B. Eberle, M.M. Mühlleitner, and P.M. Zerwas, Phys. Lett. **B505**, 149 (2001).
  - [2] V. Barger, K. Cheung, A. Djouadi, B.A. Kniehl, and P.M. Zerwas, Phys. Rev. **D49**, 79 (1994).
  - [3] D.J. Miller, eConf C010630 **P119** (2001), hep-ph/0111145.
  - [4] B. Grz̧dkowski, J.F. Gunion, Phys. Lett. **B350**, 218 (1995); A. Rouge, Phys. Lett. **B619**, 43 (2005).

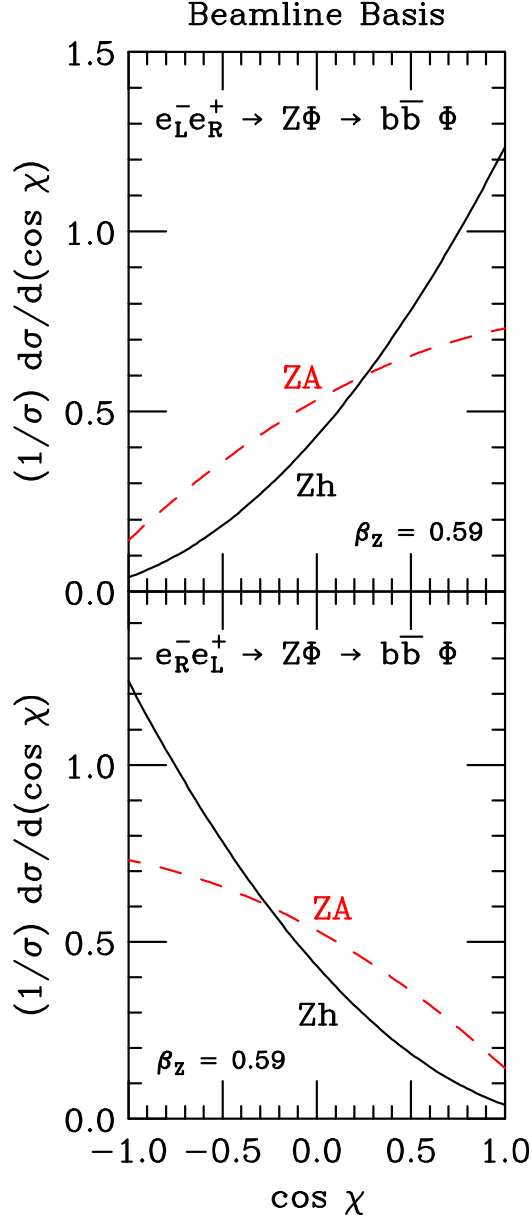


FIG. 18: Comparison of  $Z$  decay angular distributions for  $e^+e^- \rightarrow Zh \rightarrow b\bar{b}h$  and  $e^+e^- \rightarrow ZA \rightarrow b\bar{b}A$  in the beamline basis for  $\beta_Z = 0.59$  ( $M_h = 120$  GeV,  $\sqrt{s} = 250$  GeV). The decay angle  $\chi_Z$  is defined as the angle in the  $Z$  rest frame between the spin axis direction and the direction of motion of the negatively-charged lepton.

- [5] P. Nieżurawski, A.F. Żarnecki, M. Krawczyk, Acta Phys. Polon. **B36**, 833 (2005).
- [6] S. Eidelman et al., Phys. Lett. **B592**, 1 (2004).
- [7] G. Mahlon and S. Parke, Phys. Rev. **D58**, 054015 (1998).
- [8] S. Parke and Y. Shadmi, Phys. Lett. **B387**, 199 (1996).

- [9] G. Mahlon and S. Parke, Phys. Rev. **D53**, 4886 (1996).
- [10] G. Mahlon and S. Parke, Phys. Lett. **B411**, 173 (1997).
- [11] S. Parke and S. Veseli, Phys. Rev. **D60**, 093003 (1999).
- [12] Even if we don't assume the Standard Model coupling on the  $eeh$  vertex, the absence of a  $e^+e^- \rightarrow h$  signal at LEP ensures that this diagram is negligible [1].
- [13] J. Gunion, H. Haber, G. Kane, and S. Dawson, *The Higgs Hunter's Guide*, Addison–Wesley, Redwood City, CA, 1990, p. 199.
- [14] For the MSSM,  $\Lambda$  would be related to the SUSY-breaking scale and  $\eta$  would depend on the particle content appearing in the loops.
- [15] Inclusion of the finite mass effects would result in straightforward but messy modifications to Eqs. (32) and (33). These effects are greatest for  $b$ -quarks, where they are less than a few percent.
- [16] T. Inagaki, Nucl. Phys. Proc. Suppl. **37A**, 197 (1994); L. Lavoura, Phys. Rev. **D51**, 5256 (1995); Y.L. Wu and L. Wolfenstein, Phys. Rev. Lett. **73**, 1762 (1994); M. Masip and A. Rasin, Nucl. Phys. **B460**, 449 (1996); D. Bowser–Chao and D. Chang, Phys. Rev. Lett. **81**, 2028 (1998); B. Grzadkowski and J. Pliszka, Acta Phys. Polon. **B32**, 1919 (2001); R.M. Godbole, S. Kraml, M. Krawczyk, D.J. Miller, P. Nieżurawski, and A.F. Żarnecki, hep-ph/0404024; K. Kiers, M. Assis, and A.A. Petrov, Phys. Rev. **D71**, 115015 (2005); J.F. Gunion and H.E. Haber, Phys. Rev. **D72**, 095002 (2005).